To the Graduate Council:

I am submitting herewith a thesis written by Donald Neal Pittman entitled "Spectrum of Prebreakdown Light and Temporal Correlation of Prebreakdown Current and Light Pulses at a Point Cathode in Hexane." I have examined the final copy of this thesis for form and content and recommend that it be accepted in partial fulfillment of the requirements for the degree of Master of Science, with a major in Electrical Engineering.

Marshall O. Pace

Marshall O. Pace, Major Professor

We have read this thesis
and recommend its acceptance:

D. Vaughn Blalock

Ign Alexeff

Accepted for the Council:

C. W. Minkel

Vice Provost
and Dean of the Graduate School

STATEMENT OF PERMISSION TO USE

In presenting this thesis in partial fulfillment of the requirements for a Master of Science degree at The University of Tennessee, Knoxville, I agree that the Library shall make it available to borrowers under rules of the Library. Brief quotations from this thesis are allowable without special permission, provided that accurate acknowledgment of the source is made.

Permission for extensive quotation from or reproduction of this thesis may be granted by my major professor, or in his absence, by the Head of Interlibrary Services when, in the opinion of either, the proposed use of the material is for scholarly purposes. Any copying or use of the material in this thesis for financial gain shall not be allowed without my written permission.

Signature Donald Neal Pittman

Date 9-19-86

SPECTRUM OF PREBREAKDOWN LIGHT AND TEMPORAL CORRELATION OF PREBREAKDOWN CURRENT AND LIGHT PULSES AT A POINT CATHODE IN HEXANE

A Thesis

Presented for the

Master of Science

Degree

The University of Tennessee, Knoxville

Donald Neal Pittman

December 1988

ACKNOWLEDGEMENTS

I am grateful to my wife, Donna, for her support, and her aid in proofreading this thesis. I thank the members of the thesis committee, Dr. Marshall Pace, Dr. Vaughn Blalock, and Dr. Igor Alexeff, for their suggestions and discussions concerning the topics involved in this research. Alan Wintenberg also provided some important suggestions and Ken Swayne assisted in obtaining and processing some of the data and purifying the liquid sample. I also thank Dr. Randy James of Martin Marietta Energy Systems, Inc. for his help in obtaining and setting up the monochromator used in the experiments. I am indebted to the Office of Energy Storage and Distribution, Department of Energy for financing this work under contract DE-AC05-84OR21400 with Martin Marietta Energy Systems, Inc.

ABSTRACT

Prebreakdown current and light emission were investigated at a 3 micron tip radius needle cathode in hexane stressed by a dc power supply. A gap separation of 5 mm was used, producing a nominal electric field of 10^9 V/m. The spectral intensity of the light emission was measured in intervals of 10 nm for wavelengths ranging from 330 to 620 nm. Spectral peaks were detected at 430, 510, and 590 nm which corresponded to an intense spectral band at 431.25 nm produced from hydrocarbon reactions like those found in the sun s atmosphere, and a spectral line at 590 nm that is associated with hydrocarbons at high pressure. The temporal correlation of the light and current pulses was also determined. The results from the correlation suggested that the current leads the light by one to six nanoseconds. The resolution of this measurement was limited by the effective sampling period of 2.5 nsec.

TABLE OF CONTENTS

CHAPTER		PAGE
1	**INTRODUCTION**	1
	1.1 Background Information	1
	1.2 Prebreakdown Theories	2
	1.2.1 Formation of Low Density Region	4
	1.2.2 Growth of Low Density Region	5
	1.3 Light Emission Studies	7
	1.4 Objectives	7
2	**EXPERIMENTAL APPARATUS**	9
	2.1 Introduction	9
	2.2 Power Supply Filtering	9
	2.3 Current and Light Detection System for Correlation Study	11
	2.4 Current and Light Detection System for Spectral Study	17
3	**EXPERIMENTAL PROCEDURES**	22
	3.1 Introduction	22
	3.2 Liquid and Test Cell Purification	22
	3.3 Delay Measurements	24
	3.3.1 Light Detection Delay	24
	3.3.2 Current Detection Delay	28
	3.4 Obtaining Data	30
	3.4.1 Obtaining Data for Correlation Study	32
	3.4.2 Obtaining Data for Spectral Study	32

CHAPTER PAGE

4 DATA ANALYSIS AND RESULTS 33

4.1 Introduction 33

4.2 Temporal Correlation of Prebreakdown Current Pulses and Light Emission 33

4.3 Spectral Content of Prebreakdown Light Emission 44

5 CONCLUSION 54

5.1 Summary of Results 54

5.2 Suggestions for Future Research 55

REFERENCES 56

VITA 61

LIST OF FIGURES

FIGURE		PAGE
1.	Development of LDR in hexane at a point cathode ...	3
2.	Power supply filter circuit	10
3.	Current and light detection system for correlation study	12
4.	Lens setup for correlation study	15
5.	Current and light detection system for spectral content study	18
6.	Lens setup for focusing light onto monochromator ..	19
7.	Purification system	23
8.	Apparatus used to measure light detection delays ..	26
9.	Typical light pulse generated by LED and detected by PMT	27
10.	Appartus used to measure current detection delay ..	29
11.	Current and light pulses for a PMT gain of 5×10^6 at needle voltages of (a)-11 kV, (b)-13 kV, and (c)-15 kV	34
12.	Current and light pulses for a PMT gain of 2×10^7 at needle voltages of (a)-11 kV, (b)-13 kV, and (c)-15 kV	35
13.	Current and light pulses for a PMT gain of 4×10^7 at needle voltages of (a)-11 kV, (b)-13 kV, and (c)-15 kV	36
14.	Light and current pulses for a PMT gain of 5×10^6 at needle voltages of (a)-11 kV, (b)-13 kV, and (c)-15 kV	37
15.	Light and current pulses for a PMT gain of 2×10^7 at needle voltages of (a)-11 kV, (b)-13 kV, and (c)-15 kV	38
16.	Light and current pulses for a PMT gain of 4×10^7 at needle voltages of (a)-11 kV, (b)-13 kV, and (c)-15 kV	39
17.	Typical plot of a current and light pulse	41

FIGURE PAGE

18. Block diagram of processing used to determine the spectral intensity at a specified wavelength 45

19. Spectral response of PMT cathode 46

20. Integration of waveform using trapezoidal approximation 47

21. Light emission spectrum after processing 15 waveform pairs 49

22. Light emission spectrum after processing 20 waveform pairs 49

23. Light emission spectrum after processing 25 waveform pairs 50

24. Light emission spectrum after processing 30 waveform pairs 50

25. Light emission spectrum after processing 35 waveform pairs 51

26. Light emission spectrum after processing 40 waveform pairs 51

27. Effective spectral response of monochromator 53

28. Effective spectral response of monochromator when source is focused on left half of slit 53

29. Effective spectral response of monochromator when source is focused on right half of slit 53

CHAPTER 1

INTRODUCTION

1.1 Background Information

Electrical insulation is the material used as a barrier between conductors that are at different voltages or potentials. Breakdown occurs when the insulation fails to act as a barrier, allowing current to flow between the conductors. In high voltage systems this event is usually characterized by an electrical spark or arc between the conductors, resulting in damage to the system and its environment.

The study of electrical insulation can be broken down into a study of the three classifications of dielectrics--solids, liquids, and gases. Liquid dielectrics are used in electrical components such as transformers, capacitors, breakers, cables, and switchgear. In most cases, the dielectric is desired to be nontoxic, biodegradable, nonflammable, inexpensive, and resistant to breakdown.

The purpose of this study was to provide more information on the events that occur in liquid dielectrics prior to breakdown. If the prebreakdown processes could be understood, then their initiation could be inhibited, and safety instruments could be developed that would detect and interrupt the breakdown process before any damage could occur. This understanding might also give insight into

manufacturing liquid dielectrics that have a higher breakdown strength, which would allow power systems to operate at higher voltages thus increasing efficiency.

The next three sections discuss the basic theories involving prebreakdown phenomena, review previous research and present the objectives of this study. The following two chapters describe the experimental apparatus and procedures used in the research conducted, and the fourth chapter presents the results. The last chapter provides the conclusions obtained from the study.

1.2 Prebreakdown Theories

While prebreakdown events in liquids are not fully understood, progress has been made in the past that has lead to an understanding of the physical processes involved on a macroscopic level [9,14,32]. By using such optical techniques as the Schlieren method [6,11,18], several researchers have found that a bush-shaped region having a different index of refraction than the surrounding liquid will form at the electrode in an electrically stressed liquid dielectric. If the applied stress is large enough, this region will grow until it forms a channel between the cathode and anode causing breakdown to occur. The region is thought to be a gaseous phase since the formation and growth of this "streamer" can be inhibited by pressurizing the liquid [8,21,26]; hence, it is often referred to as a low density region (LDR). A sequence of shadowgraphs in Fig. 1

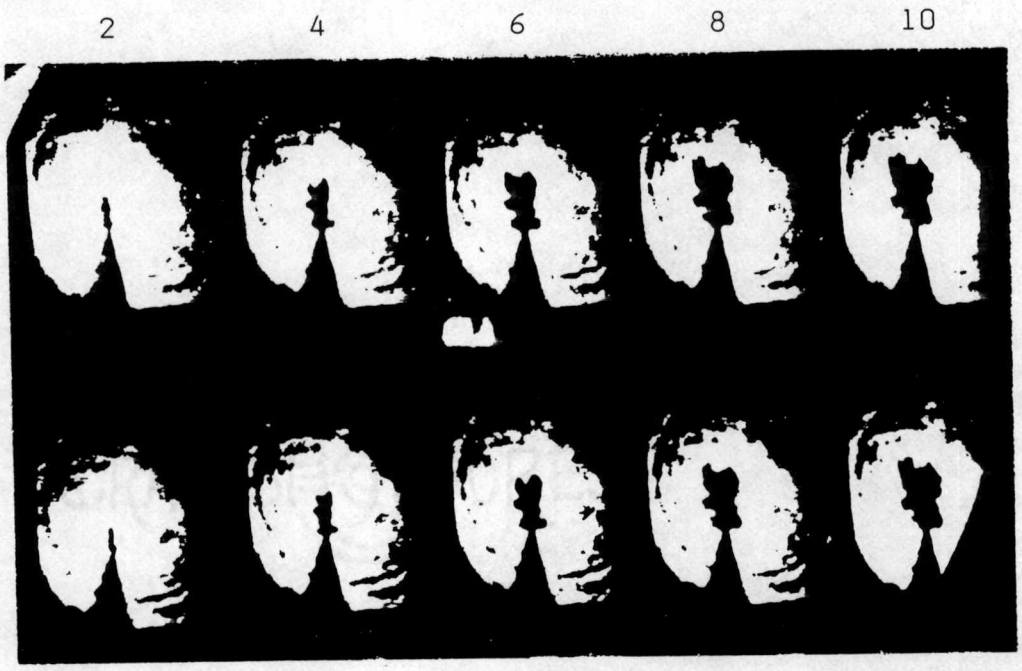

Fig. 1: Development of LDR in hexane at a point cathode

show the development of a LDR on the tip of a 3 micron tip radius needle cathode in hexane [23]. In these photos the LDR is the black bush-shaped region and the needle is the black triangle. The other patterns in the photos are due to the laser illumination used in the experiment. There are several different theories, which will be reviewed in the following subsections, that attempt to explain the underlying mechanisms in the formation and growth of a LDR.

1.2.1 Formation of Low Density Region

While there are different views about the formation of LDRs, most researchers agree that a charge injection process is involved. These different views are presented in the following paragraph.

Forster [13] has suggested that favorable sites on the cathode such as grain boundaries, whisker-like protrusions, or dust particles, enhance the local electric field by a factor of 100 to 300, which causes electrons to be injected into the liquid, pushing the liquid away from the cathode and forming a LDR. Using the Kerr-effect to observe the electric field near a point cathode and to infer charge motion, Kelley and Hebner [20] have concluded that a channel (possibly due to the same asperities as described by Forster) forms which conducts charge into the liquid, causing joule-heating to occur. They have estimated this energy to be on the same order as that required to vaporize the liquid and thus form a LDR. However, Thomas [33]

developed a computer model that solved for the motion of charges injected from a cathode surface into a liquid and found that the temperature increase from joule-heating was not enough to form a cavity due to vaporization. Alexeff [1] has suggested that charge injected from the cathode is trapped near the surface of the interface and, then coulomb force, which could be has high as 20 atmospheres, causes the liquid surface to be pushed away from the electrode forming a LDR.

1.2.2 Growth of Low Density Region

Recently a combined effort of The National Bureau of Standards and The University of Tennessee [23] has shown that prebreakdown current pulses occur only when a LDR exists. Yamashita and Amano [41] and Alexeff et al. [2] have shown that prebreakdown light emission has the same shape as a LDR. Also, Wintenberg et al. [36,37] have observed that current pulses occur in bursts where each burst consists of pulses that increase approximately linearly in amplitude. These current pulses were correlated with light pulses detected by a photomultiplier tube.

Alexeff et al. [1] have developed the following model that seems to explain these phenomena. When the LDR is formed, the cavity surface is at the same potential as the cathode; but as the LDR expands due to coulombic pressure, the potential of the cavity surface decreases because the charge on the surface is being spread over a greater

surface area. This potential difference continues to increase until the critical field of the LDR is reached, causing breakdown to occur inside the cavity which results in a current pulse and light emission. The charge transferred during this breakdown will increase the potential of the LDR surface back to that of the cathode. This sequence of events will continue to repeat until the coulombic pressure, which is decreasing as the LDR grows, is equal to the ambient pressure. As the net pressure decreases, instabilities [35] of the LDR will either cause the cavity to break up or produce a secondary streamer [10] that crosses the remaining gap and results in total breakdown. Pace [27] has combined this model with one developed by Watson [35] to simulate the same current pulse behavior as seen by Wintenberg et al. [39] in several experiments. This theory does, however, contradict observations made by Kelley and Hebner [19] that imply the LDR surface is always at the same potential as the cathode. If the LDR is considered to be a sphere of radius b and a needle cathode is radius c, then the electric field at the needle tip is

$$E = V/(c - c^2/b) , \qquad (1\text{-}1)$$

where V is the potential difference between the LDR surface and the needle tip. Assuming the LDR radius to be 25 microns and the effective needle radius to be 0.1 microns as Forster has suggested [13], then the potential difference required for an electric field of 10^9 V/m that would induce field emission [29] is 100 volts. This potential difference

might be too small to resolve using Kelley and Hebner's technique [19]. Therefore, Pace [27] and Alexeff [1] may not be contradicting Kelley and Hebner [19].

1.3 Light Emission Studies

Previous measurements of prebreakdown current and light emission made by Hanna et al. [17], Kelley et al. [22], and Morikawa [24] have not allowed the actual temporal correlation of the two signals to be determined because of the lack of sensitivity and bandwidth in their detection systems [38].

The few researchers that have measured the spectrum of light emitted [24,25,30,40] did not concentrate on prebreakdown, but on breakdown. During breakdown, temperatures can exceed 1400 ^{o}K [11], which can drastically affect the spectral content of the light emitted.

1.4 Objectives

To study the prebreakdown phenomena at a point cathode in liquid hexane, the research reported in this thesis has combined a low-noise, wide-band preamplifier designed by Blalock [4] to detect prebreakdown current pulses; a high-gain photomultiplier tube (PMT) to detect prebreakdown light pulses; and a monochromator to observe the light spectrum to accomplish the following objectives.

1) Determine, for the first time, the actual temporal

correlation of the prebreakdown current and light pulses.

2) Determine, for the first time, the spectral content of the prebreakdown light emission.

Showing the light and current to be correlated would support the theory developed by Alexeff et al. [1], and determining the actual delay between the two events would provide some information on the characteristics of the molecules present in the LDR. The light emission spectrum could be used to determine the types of gases present in the LDR.

CHAPTER 2

EXPERIMENTAL APPARATUS

2.1 Introduction

The basic method used, in studying the spectrum of prebreakdown light emission and temporal correlation of the light and current, was to apply a high voltage to a needle cathode immersed in liquid hexane, while detecting the image current in a plane anode (using a low noise amplifier), and detecting the light emission (using a photomultiplier tube). Hexane was chosen as the liquid to study because it is one of the major constituents in transformer oil.

The following section describes in detail how the high voltage was applied to the needle, while the last two sections discuss the apparatus used in determining the temporal correlation and spectral content of the light.

2.2 Power Supply Filtering

To eliminate the effect of power supply ripple on the events occurring at the needle, to limit the amount of current supplied in the event of a breakdown, and to provide a means of measuring the voltage on the needle, a filter circuit was constructed as shown in Fig. 2. Resistor R_1 and capacitors C_1 and C_2 formed a single pole lowpass filter with a 3 db bandwidth of 1.4 Hz. This filter would attenuate the 20 KHz component of the ripple from the the

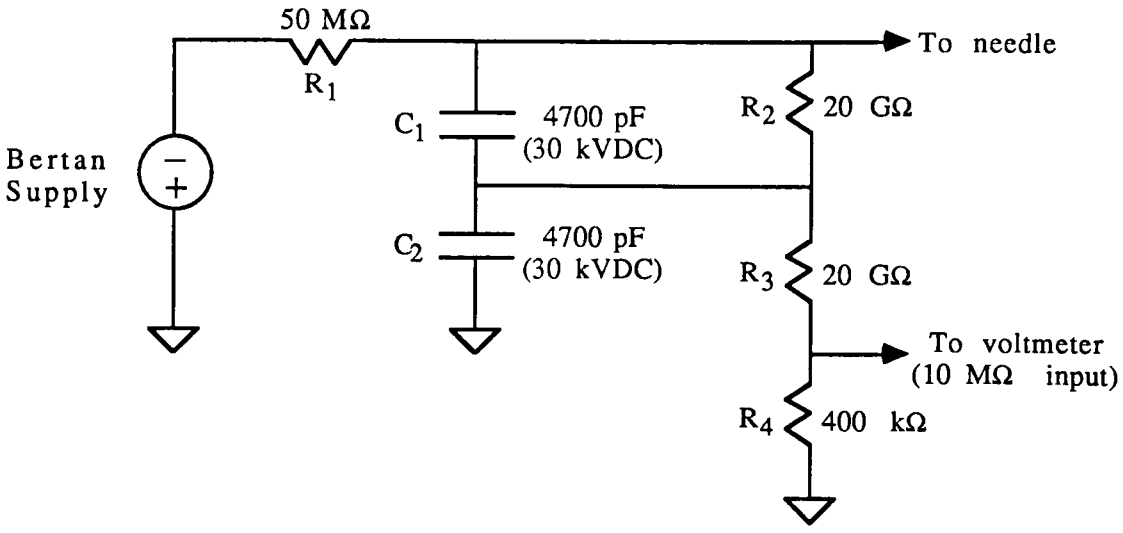

Fig. 2: Power supply filter circuit

power supply by 83 db. Resistor R_1 would also limit the supply current to about 0.2 mA if a breakdown occurred. The 100,000:1 voltage divider consisting of R_2, R_3, and R_4 allowed a 10 megohm input impedence voltmeter to be used to measure the voltage on the needle. The connection from the middle of the voltage divider to the common node of the capacitors assured the charge distribution of the capacitors was equal. The capacitors C_1 and C_2 would hold 35.25 microcoulombs of charge for a high voltage of -15 kV. For a typical prebreakdown discharge of 150 picocoulombs, the high voltage would theoretically be reduced to only -14.99994 kV. The components were chosen such that the overall voltage rating of the circuit was in excess of 60 kVDC. The filter circuit was mounted on a Plexiglas platform and placed in a stainless steel box that was mounted on the bottom of the test cell. To prevent corona discharge in the filter circuit, all of the circuit nodes were made smooth and placed so that no two nodes were within two inches of each other, and the box was filled with mineral oil.

2.3 Current and Light Detection System for Correlation Study

The basic experimental setup used for detecting prebreakdown current and light pulses is shown in Fig. 3. The four-inch, stainless steel, cubical, test cell was equipped with a pair of two-inch diameter, glass viewports; a 1.5 cm diameter, stainless steel, plane anode; and a 3

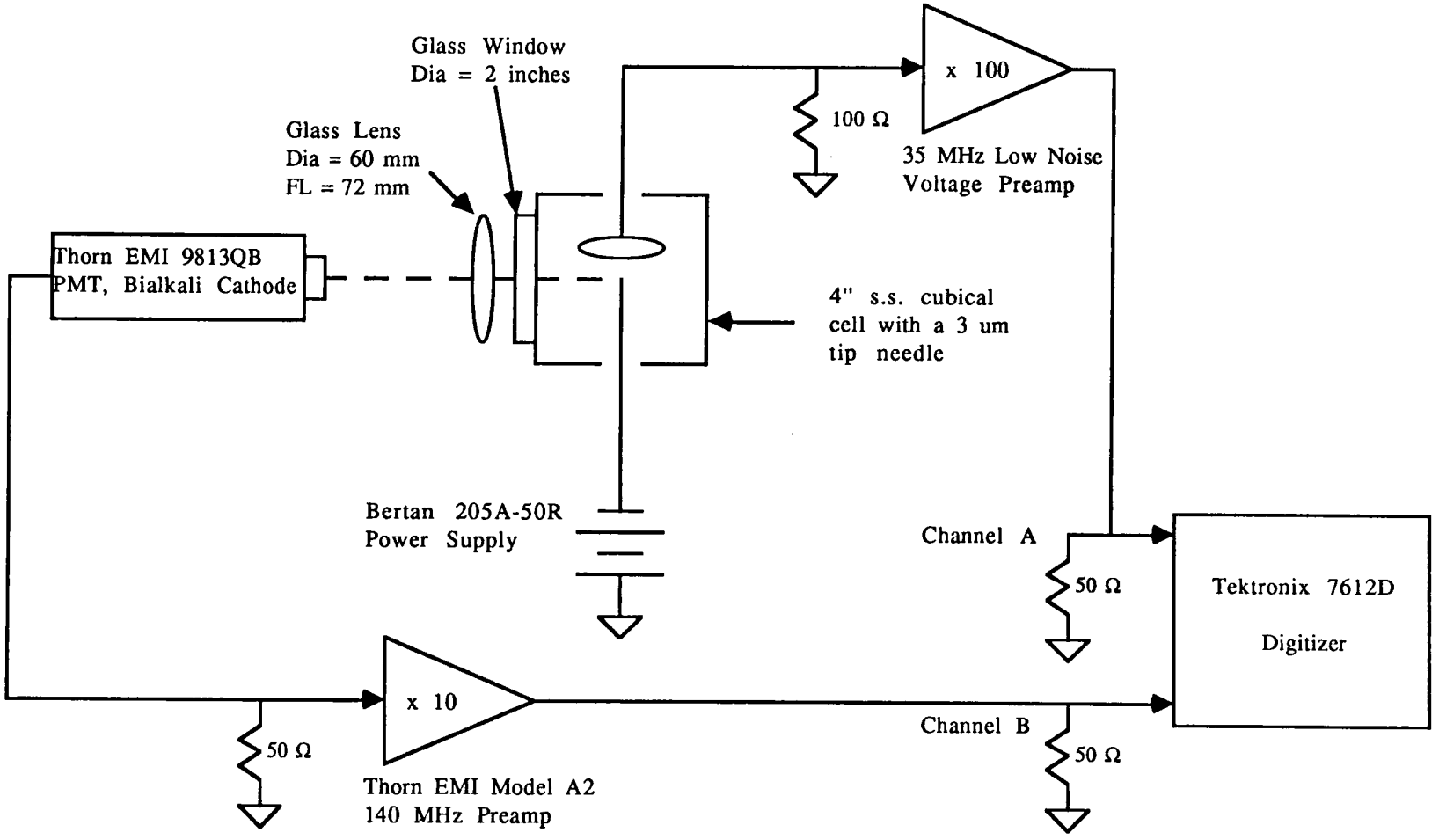

Fig. 3: Current and light detection system for correlation study

micron tip radius, steel needle cathode. A Bertan 205A-50R power supply was used to apply the negative dc stress. For the tip-plane configuration, Coelho and Debeau [5] found that the magnitude of the electric field at the needle tip was given by

$$E = V/[r \ln(2(a/r)^{1/2})] , \qquad (2\text{-}1)$$

where V = high voltage,

a = gap between needle tip and plane,

and r = tip radius.

For the gap of 5 mm used in this experiment and an applied voltage of -15 kV, the electric field at the needle tip was calculated from (2-1) to be 1.14×10^9 V/m.

A discharge at the needle would immediately produce charge movement in the anode via the electric field. This image current detected by the plane anode was converted to a voltage by a 100 ohm resistor and amplified by a 35 MHz, low-noise (0.91 nV/(Hz)$^{1/2}$), voltage preamplifier [4]. The preamplifier was mounted directly to the test cell and connected to a low capacitance feedthrough (5 pF) to reduce the RC time constant at that node. The preamplifier input impedance of 100 ohms in parallel with the 15 picofarads due to the test cell, feedthrough, and preamplifier capacitance limited the bandwidth to 106 MHz. Approximating the overall time constant of the system by combining the dominant time constant of the preamp, τ_p, and detection impedance, τ_d, as

$$\tau = \sqrt{\tau_p^2 + \tau_d^2} , \qquad (2\text{-}2)$$

resulted in an overall bandwidth of approximately 33 MHz. The equivalent input current noise was measured to be 89 nA

rms. For a signal to noise ratio of five, the minimum detectable current would be 445 nA rms.

A Thorn EMI 9813QB, photomultiplier tube (PMT) with a 2 cm, bialkali cathode and 14 stages of dynodes, transformed the light signal into a current that could be detected by a 50 ohm resistor and amplified by the Thorn EMI Model A2, 140 MHz preamplifier. The PMT was housed in a Thorn EMI FACT III cooler capable of reducing the temperature to -30 ^{o}C. To eliminate the detection of external light sources, the PMT, lens, and test cell were placed inside a light-tight optical box.

Two RG-58 coaxial cables were then used to connect the output of each preamp to the 7A16P plug-in amplifiers on the Tektronix 7612D digitizer, where each input was terminated with 50 ohms. A Tektronix 4041 computer was used to control the digitizer and power supply using an IEEE 488 bus.

A 60 mm diameter glass lens with a focal length of 72 mm was used to focus the needle tip onto the PMT as pictured in Fig. 4. The effective distance to the object as seen by the lens was closer than the actual distance of 10.5 cm, because the different indices of refraction caused the light rays to bend at the hexane-window-air interface. Neglecting the thin glass window, the law of refraction [15] gives the relationship

$$n_h \sin\theta_h = n_a \sin\theta_a \ . \qquad (2\text{-}3)$$

Also from Fig. 4,

$$\sin\theta_a = b/a' \qquad (2\text{-}4)$$

and

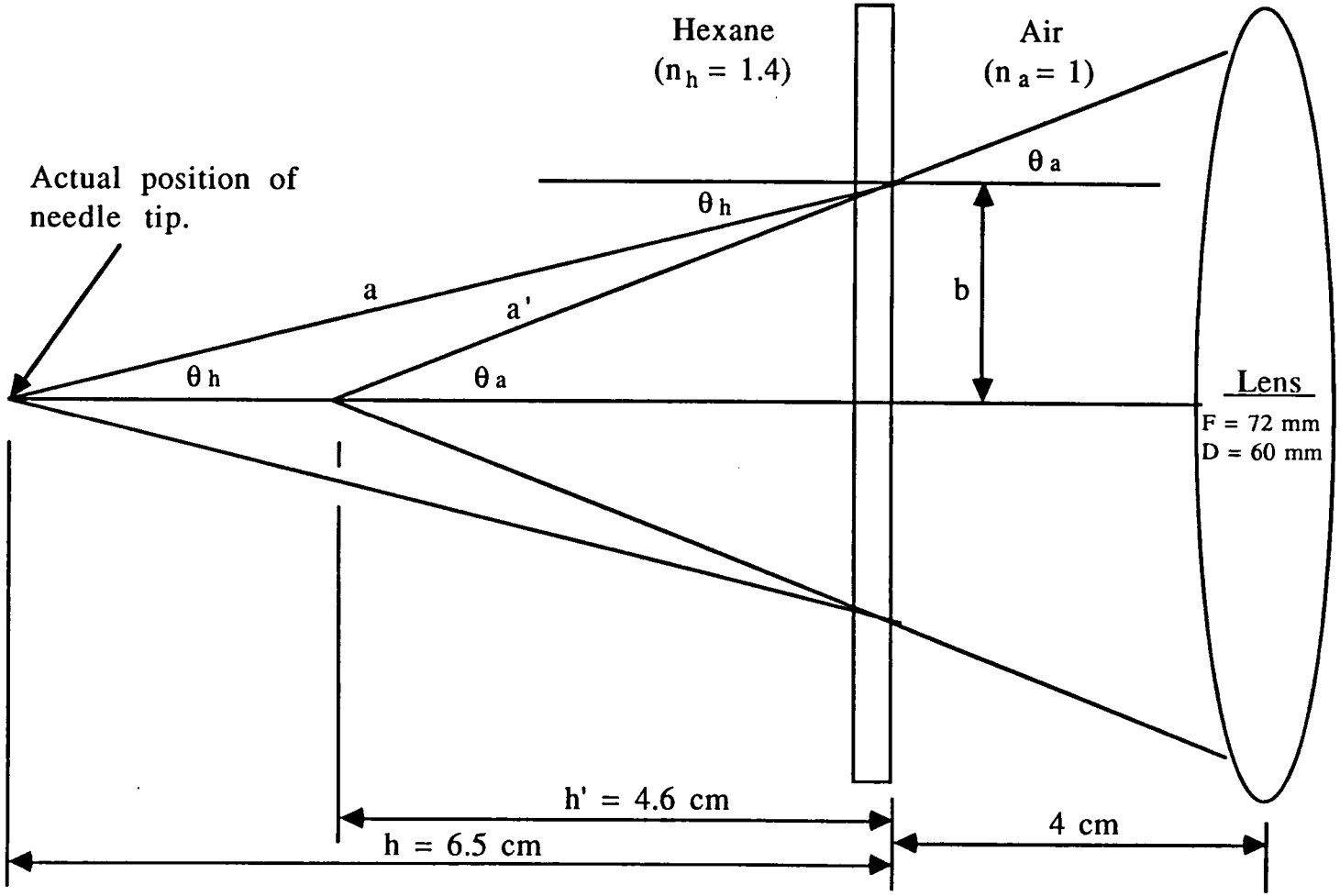

Fig. 4: Lens setup for correlation study

$$\sin\theta_h = b/a \ . \qquad (2\text{-}5)$$

Substituting (2-4) and (2-5) into (2-3) results in

$$n_a a = n_h a' . \qquad (2\text{-}6)$$

In the limit as the dimension b approaches zero, h' equals a', and h equals a, so that for small angles of incidence

$$h' = h(n_a/n_h) \ . \qquad (2\text{-}7)$$

Applying the appropriate values to (2-7) gives h' equal to 4.6 cm. The lens was mounted as close to the test cell window as possible to maximize the percentage of light detected. This placement made the effective distance to the object equal to 8.6 cm. The simple lens law,

$$1/F = 1/I + 1/O \ , \qquad (2\text{-}8)$$

where

F = Focal length of lens

O = Distance from lens to object

and

I = Distance from lens to image,

was used to determine the distance from the lens to the PMT cathode. The distance, I, that was needed was found to be 44 cm. This setup resulted in a magnification of about five. The amount of light collected by the lens was approximately 3.0% of the total light emitted, assuming an isotropic point source at the needle and neglecting any transmission losses through the hexane, window, and air.

2.4 Current and Light Detection System for Spectral Study

The experimental setup for determining the spectral content of the prebreakdown light emission was similar to that used in the correlation study except for the current detection impedence, lens setup, and the addition of a PRA model B204 UV-V monochromator. This new setup is pictured in Fig. 5.

Since the data processing technique used in finding the light spectrum consisted of integrating the current, the bandwidth of the current detection system could be lowered without affecting the results. The detection impedance was changed to 13 ohms in parallel with 3300 picofarads, which limited the bandwidth to about 3.7 MHz and decreased the current to voltage gain to 13 ohms. By decreasing the bandwidth and the gain, the pulses at the input to the low noise voltage preamplifier were made smaller in amplitude (and greater in duration) so that the preamplifier output would not saturate for large current pulses. The input current noise for this circuit was measured to be 75 nA rms.

The spectral resolution of a grating monochromator is partially determined by the number of effective grooves used on the grating, so that the maximum resolution is obtained when the grating is fully illuminated [31]; however, if the grating is over-filled the intensity of the light at the exit slit is reduced. To determine the placement of the lens that would fully illuminate the grating, Fig. 6 is considered. The effective distance from the entrance slit to the grating is 200 mm, and the dimensions of the grating

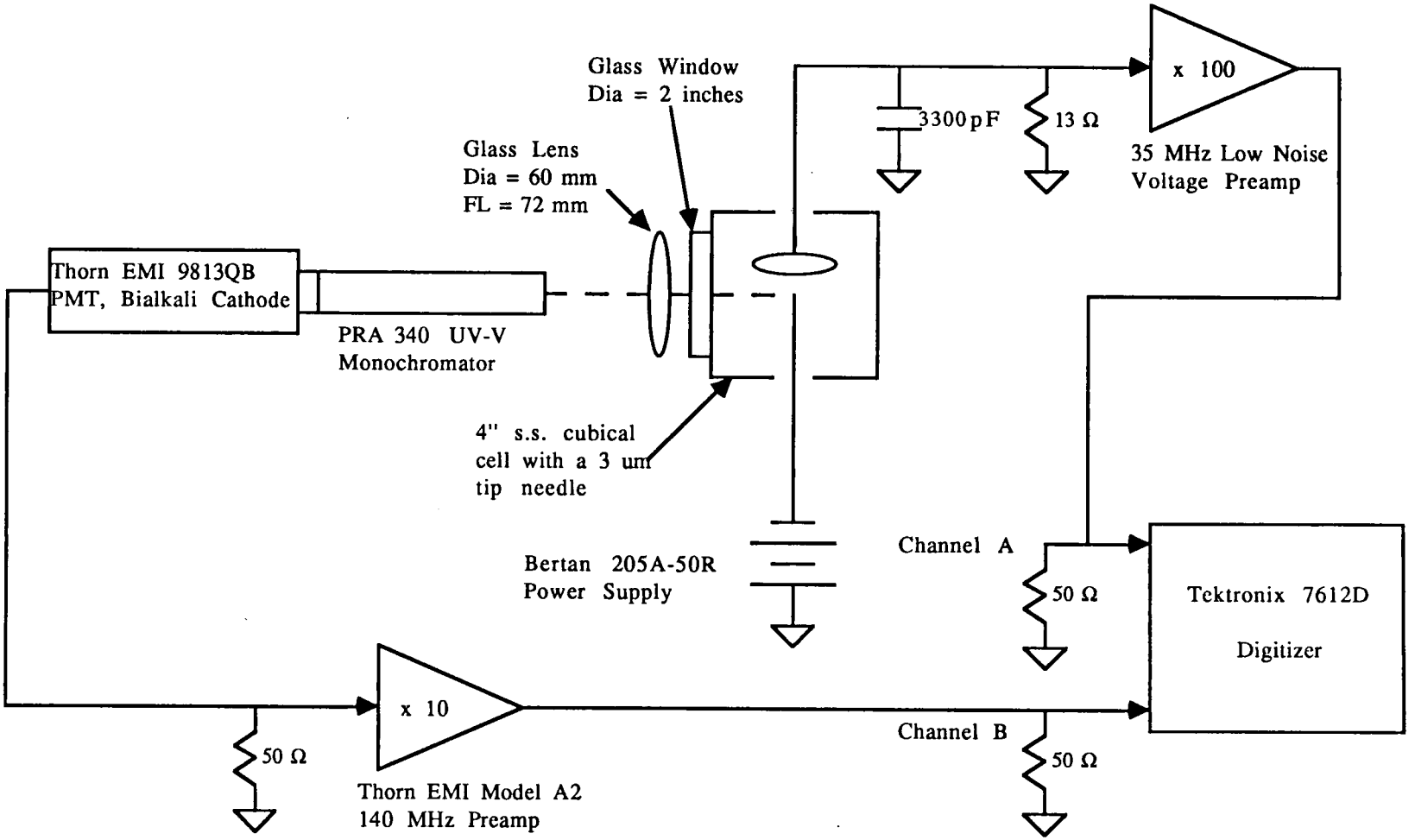

Fig. 5: Current and light detection system for spectral content study

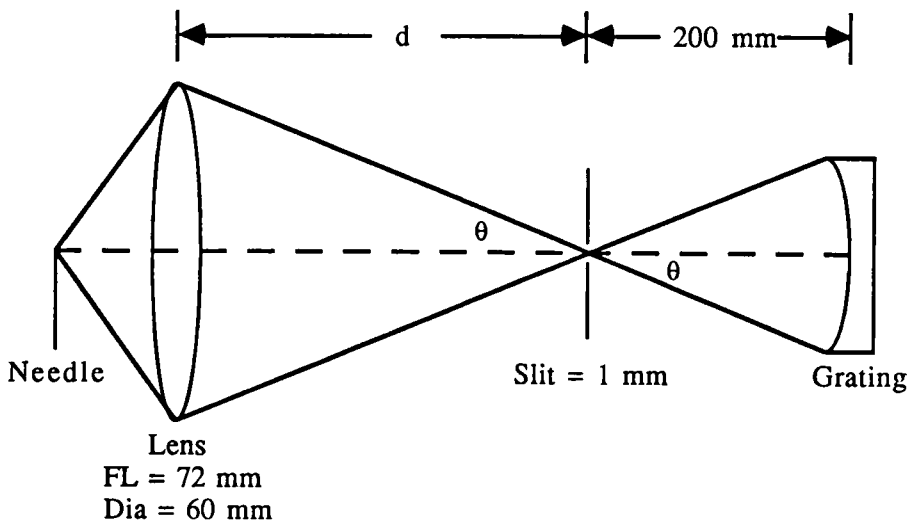

Fig. 6: Lens setup for focusing light onto monochromator

are 40 x 45 mm. If the image at the needle point is focused at the plane of the slit, then the cones of light entering and exiting the slit will be at the same angle, θ, relative to the center line of the system. For the grating to be full of light the angle θ should be

$$\theta = \tan^{-1}(22.5 \text{ mm}/200 \text{ mm}) , \qquad (2\text{-}9)$$

or 6.4^{o}. So the distance from the slit to the lens should be

$$d = (30 \text{ mm})/\tan(6.4^{o}) \qquad (2\text{-}10)$$

or 270 mm.

To be sure that the grating was not over-filled the actual distance from the slit to the lens was set at 365 mm. At this distance 73% of the grooves on the grating were covered. If all of the grooves on the grating were used, the linear dispersion would have been 4 nm/mm, but using just 73% of the grooves resulted in a linear dispersion of 5.5 nm/mm. Therefore, using 1 mm slits provided a bandpass of 5.5 nm. The monochromator's calibration was verified using the mercury vapor lines at 312.9, 334.1, 365.4, 404.7, and 435.8 nm and the helium-neon laser line at 632.8 nm.

This placement of the lens also provided a magnification of 4.7, and the typical width of the LDR at its full extent is only about 40 to 100 microns [27]; thus, the low density region (LDR) could grow to about 200 microns width before the source of light would be clipped by the entrance slit, assuming the needle image was perfectly

centered on the slit. The percentage of light collected by the lens was 2%, assuming a uniform point source at the needle and neglecting transmission losses.

CHAPTER 3

EXPERIMENTAL PROCEDURES

3.1 Introduction

The following sections describe the procedures and methods used in preparing the liquid and test cell, measuring detection delays, and obtaining the data used in both studies.

3.2 Liquid and Test Cell Purification

To reduce the possible effects of contaminants on the experimental results, the test cell and liquid were thoroughly cleaned using the purification system diagrammed in Fig. 7. All of the vessels, lines, and valves in the system were made of stainless steel. The test cell was flushed for more than four hours with ethanol being filtered by 10, 0.6, and 0.2 micron in-line filters. After this flushing, the ethanol was cyrogenically pumped out of the test cell by freezing an evacuated reservoir and warming the test cell. A Welch Scientific mechanical pump in combination with a Torr Vacuum Products model R-420 silicone oil diffusion pump was then used to evacuate the cell to approximately 1×10^{-5} Torr.

The liquid was purchased as 99.9% pure hexane and then purified further using the following procedure. The hexane was frozen using liquid nitrogen, leaving some of the

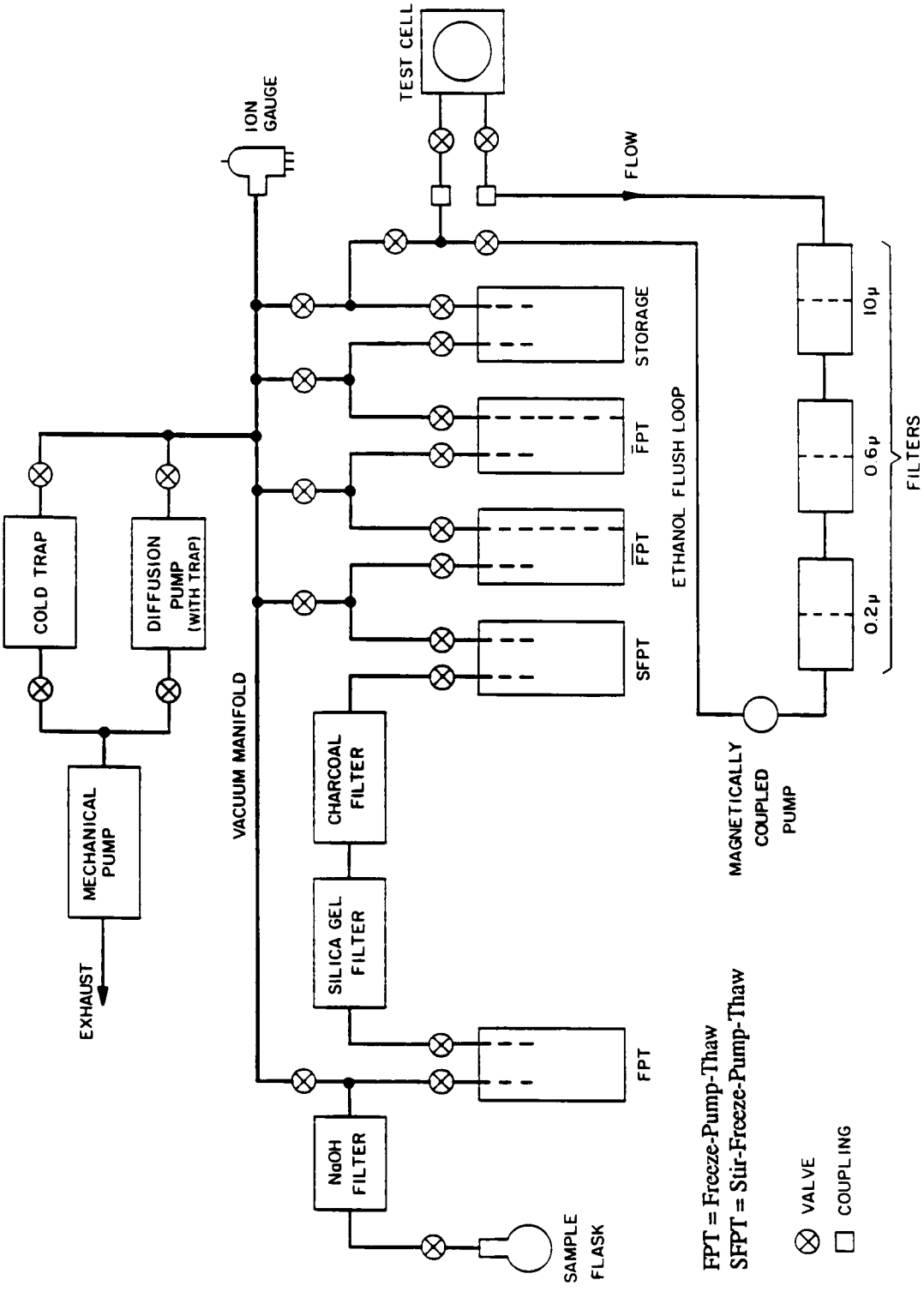

Fig. 7: Purification system

dissolved gases such as oxygen, nitrogen, and hydrogen in the liquid or gaseous state so they could be pumped away. To extract any remaining gases trapped in the frozen hexane, the liquid was thawed and even stirred at two stages and frozen again. This freeze-pump-thaw (FPT) procedure was repeated at each stage. Silica gel and charcoal filters were used to remove any moisture, while a NaOH filter was used to eliminate any CO and CO_2 in the liquid sample. Transferring the hexane from vessel to vessel was accomplished by warming the present stage and cooling the following stage with liquid nitrogen. The final transfer to the evacuated test cell was achieved by only warming the last stage of the liquid purification system while the test cell remained at room temperature.

3.3 Delay Measurements

To determine the temporal correlation of the light and current signals during prebreakdown, the propagation delays of both the light and current detection systems had to be measured. The following two subsections describe the procedures used in measuring these delays.

3.3.1 Light Detection Delay

The same basic experimental setup used for detecting prebreakdown light emission was also used to determine the light signal delay through the air, PMT, cable, and PMT

preamp. This setup is shown in Fig. 8. The light-emitting diode (LED) in conjunction with the HP 215A pulse generator, which is capable of producing a voltage pulse with a one nanosecond rise-time, was used to simulate the prebreakdown light pulses. The 5 ohm resistor in the LED circuit was used to limit the current to about 200 mA, while the 50 ohm resistor was used to match the cable impedance when the LED was not conducting. The rise-time of the voltage across the LED for a 2.5 volt pulse input to the circuit was measured to be 3 nanoseconds. This setup produced approximately an eight nanosecond rise-time pulse (depending on the PMT gain) out of the PMT preamp, which was comparable to the rise-time of the prebreakdown light pulses. Fig. 9 is a typical plot of a light pulse generated by the LED circuit as detected by the PMT. By using a dc power supply, the voltage across the LED needed to produce light was found to be 1.5 volts. Assuming the LED light pulse began when V_{LED} reached 1.5 V, the light detection delay was measured as the difference between the time when V_{LED} equaled 1.5 volts and the time when $V_{(PMT\ PREAMP)}$ equaled 2% of the peak value. This measurement was made for three different gain settings on the PMT as outlined in Table 1. Each delay was measured at three different times with no deviation from the values in Table 1.

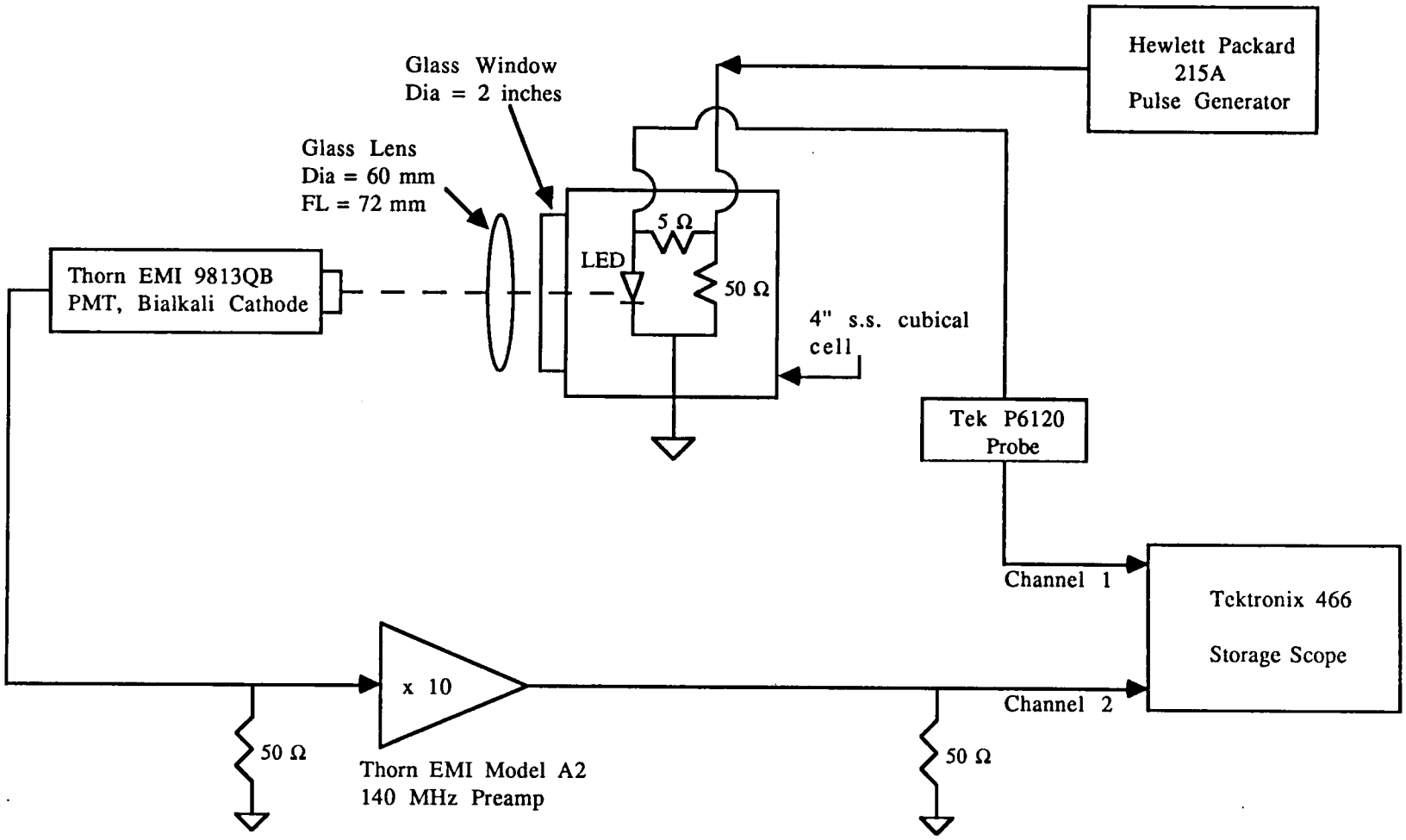

Fig. 8: Apparatus used to measure light detection delays

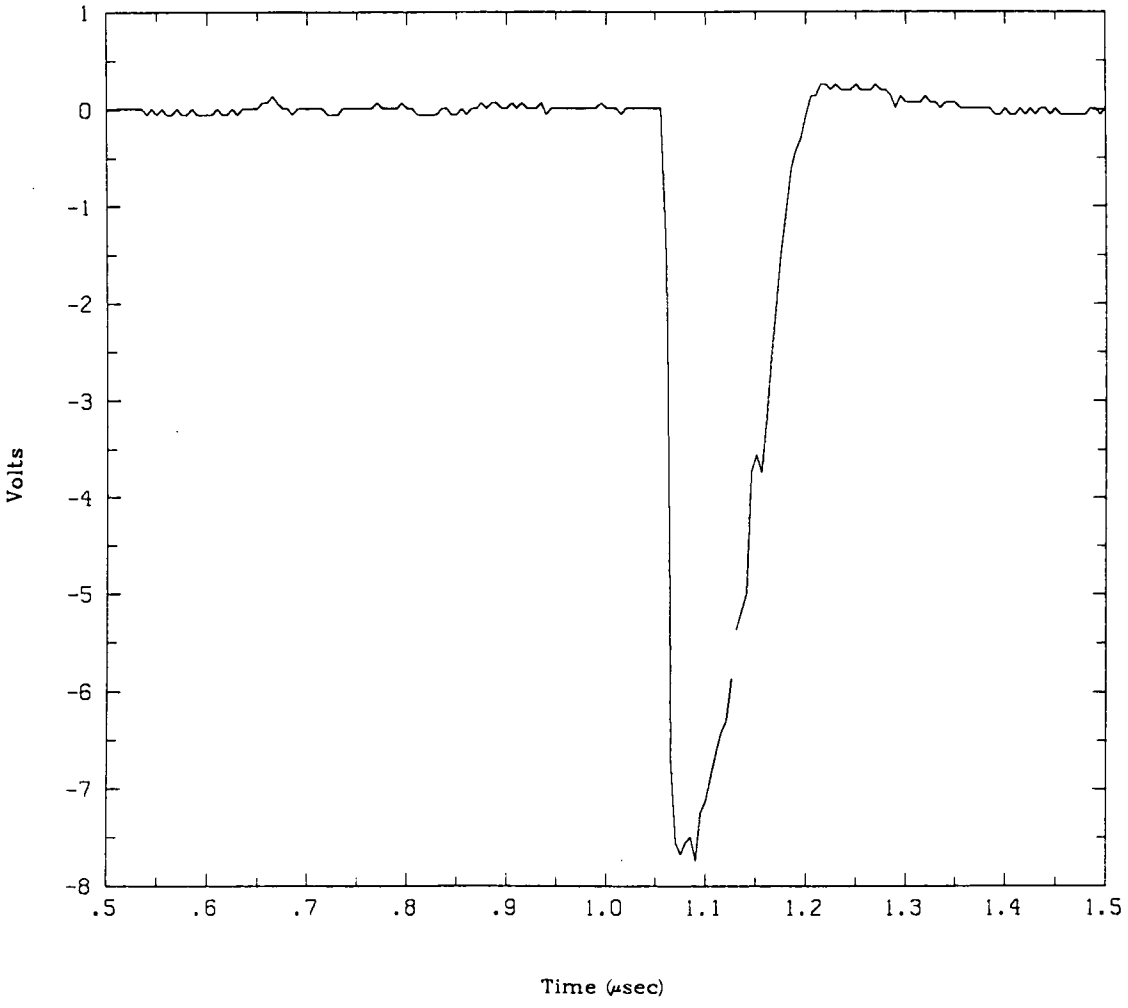

Fig. 9: Typical light pulse generated by LED and detected by PMT

Table 1

Light detection delays

PMT Gain	Delay (ns)	PMT Output Rise-time (ns)
5×10^6	71	8
2×10^7	65	7
4×10^7	62	6

3.3.2 Current Detection Delay

The apparatus used in measuring the current detection delay is shown in Fig. 10. The voltage divider was added to the input of the low noise voltage preamplifier to attenuate the signal from the HP 215A. The resistor R_2 was mounted on the preamp circuit board through a grounded copper shield to reduce the parasitic capacitance parallel to the resistor, which prevented voltage peaking at the input to the preamp. Cable #1 was the same cable that was used in the detection setup (Fig. 3 p. 12) to connect the output of the preamp to the digitizer. The procedure used to determine the propagation delay through the low noise voltage preamplifier and cable consisted of two steps. First, the trigger output and pulse output of the HP 215A were synchronized, using the variable delay adjustment on the HP 215A, so that both signals reached 2% of their peak values at the same time. Second, the pulse output was connected to the input of the preamp, and the delay was measured as the difference between

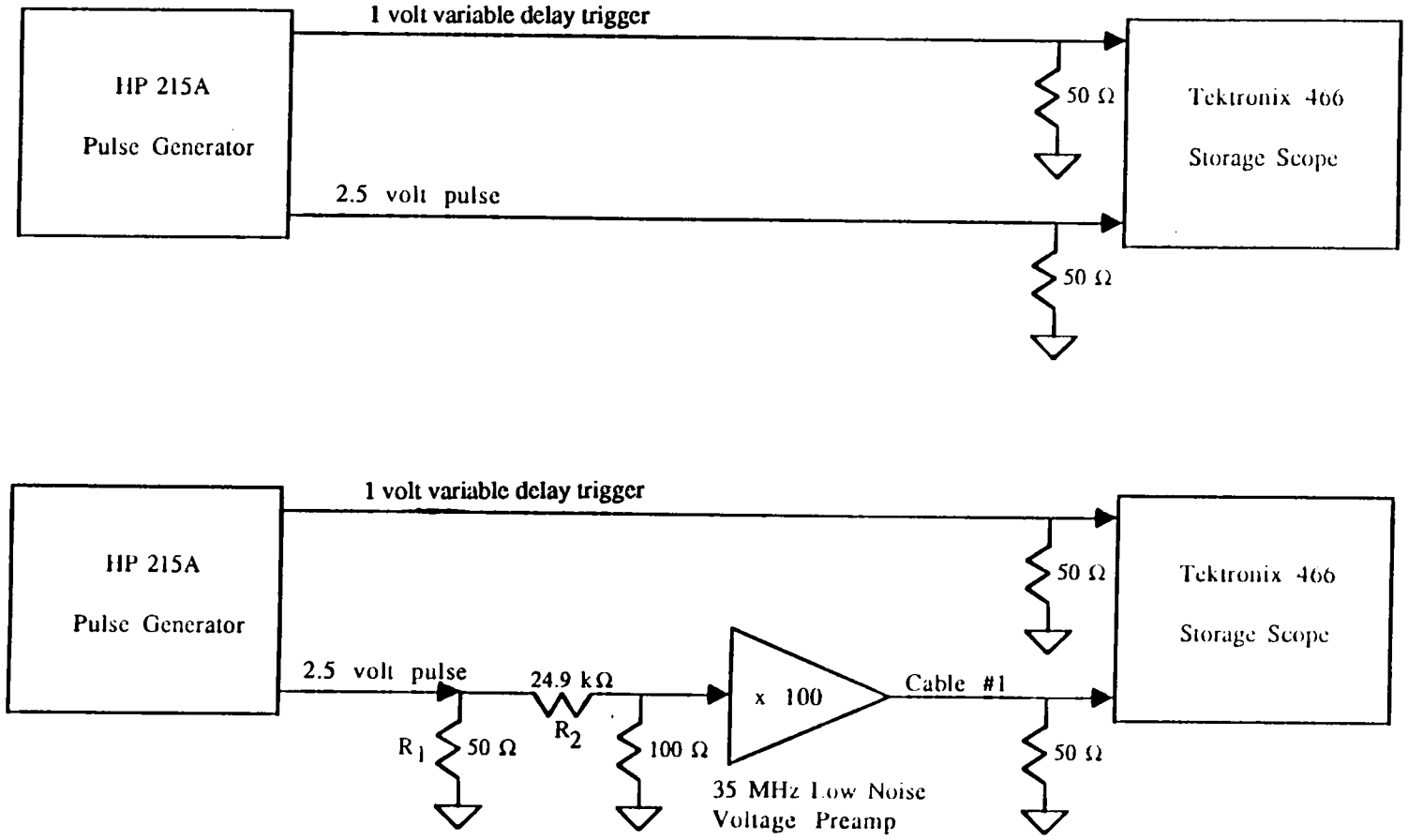

Fig. 10: Appartus used to measure current detection delay

the time it took the trigger pulse to reach 2% of its peak value and the time it took the preamp output to reach 2% of its peak value. This two-step procedure was necessary to avoid loading the input of the preamp with probe or cable capacitance. The propagation delay was found to be 18.5 nanoseconds. The only delay that was not accounted for in this measurement was the time that it took for charge motion in the liquid to appear as a voltage across the 100 ohm input resistance of the preamp. This delay was calculated from

$$t = u_1 d_1 + u_2 d_2 \ , \qquad (3\text{-}1)$$

where u_1 = speed of light in hexane (2.1×10^8 m/s),

u_2 = speed of light in metal (3.0×10^8 m/s),

d_1 = distance from needle cathode to plane anode (5 mm),

and d_2 = distance from plane anode to 100 ohm resistor (14 cm),

resulting in

$$t = 0.5 \text{ nanosecond} \ . \qquad (3\text{-}2)$$

Adding this value to the measured value of 18.5 nanoseconds resulted in a 19.0 nanosecond propagation delay of the current detection system.

3.4 Obtaining Data

Using the appropriate detection system for the correlation and spectral studies as described in sections 2.2 and 2.3, both the current and light signals were

digitized at a rate of 200 MHz, where each channel recorded 2048 data points. This procedure produced a waveform for each channel that was 10.24 microseconds long with 5 nanoseconds between the data points. A Tektronix 4041 computer was used to control the digitizer and power supply, using an IEEE 488 bus, and to process the data.

The PMT was cooled to -23 ^{o}C for the correlation setup and -28 ^{o}C for the spectral setup. In both cases the PMT dark count, due to the thermal excitation of electrons on the cathode or dynodes and stray background light, was never above 1000 pps. Considering the dark counts to be a Poisson process, the probability of no dark counts occurring in some interval t_a was

$$P(\text{no counts in interval } t_a) = \exp(-\Delta t_a) , \qquad (3\text{-}3)$$

where Δ was the average rate of occurrence. For the worst case rate of 1000 pps, this probability for a 10.24 microsecond interval was 98.98%. Therefore, the chance of capturing a dark count in a waveform was small. Another source of noise was noticed, however, for PMT gains greater than or equal to 2×10^7. A large pulse of light would generate much smaller pulses that occurred within a microsecond after the large pulse. This "after pulsing" effect was negligible for the data obtained in the spectral study because the light pulses were not large enough.

3.4.1 Obtaining Data for Correlation Study

Twelve waveform sets of light and current were obtained and stored on a disk for needle voltages of -11, -13, and -15 kV, each at PMT gains of 5×10^6, 2×10^7, and 4×10^7. The waveforms were then interpolated so that the time between consecutive data points was 2.5 nanoseconds. Aliasing that occurred during the sampling process was noticed in the interpolated light waveforms, but not in the current waveforms.

3.4.2 Obtaining Data for Spectral Study

The needle high voltage was set at -16 kV and the PMT gain at 8×10^7 for all the data obtained. Eight spectral sweeps of data were taken where one spectral sweep consisted of five waveform sets of light and current at each of thirty different wavelengths of light ranging from 330 nm to 620 nm in intervals of 10 nm. Since the monochromator bandpass was 5.5 nm there were gaps of 4.5 nm in the spectrum that were not measured.

CHAPTER 4

DATA ANALYSIS AND RESULTS

4.1 Introduction

This chapter discusses the details involved in analyzing and determining the results of the correlation and spectral content studies. One section is devoted to each study, providing information on the data processing techniques and the evaluation of the results. Possible sources of error and their significance are also discussed.

4.2 Temporal Correlation of Prebreakdown Current Pulses and Light Emission

The waveforms obtained in the correlation study were much like those seen by Wintenberg et al. [36,37,39] and Hanna et al. [17], except for the higher bandwidth and lower noise used in the experiments here. The plots in Figs. 11-16 compare typical waveforms of prebreakdown current and light for the three different high voltages and PMT gain settings used in the experiment. Figs. 11-13 focus on the small early pulses in a burst while Figs. 14-16 concentrate on the large pulses. The light waveforms have been scaled to have the same magnitude range as the current, and shifted by adding a dc offset. These plots have been adjusted for the current detection delay (19 ns) and the light detection delay (62-71 ns). The width of a current pulse at 50% of

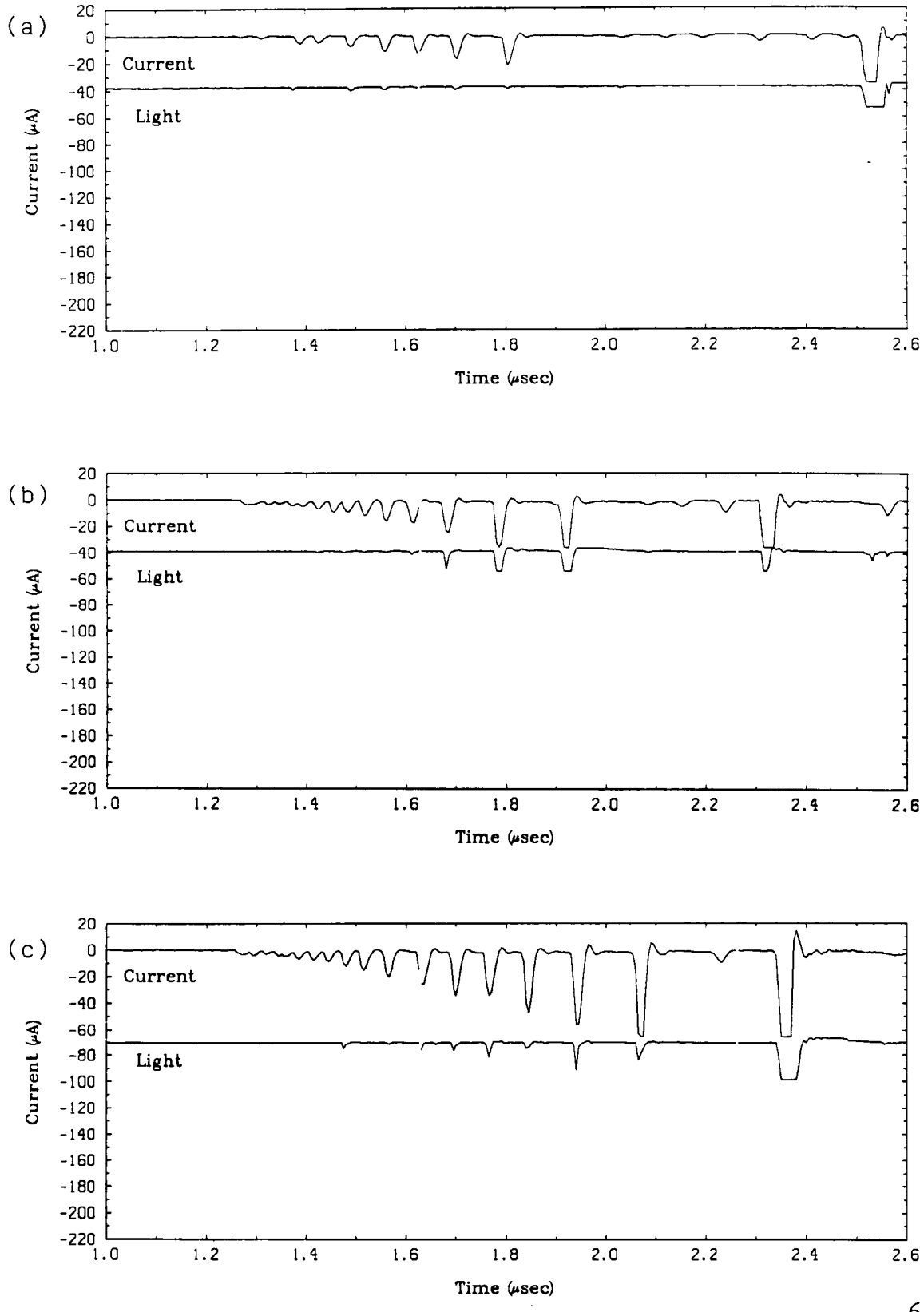

Fig. 11: Current and light pulses for a PMT gain of 5×10^6 at needle voltages of (a)-11 kV, (b)-13 kV, and (c)-15 kV

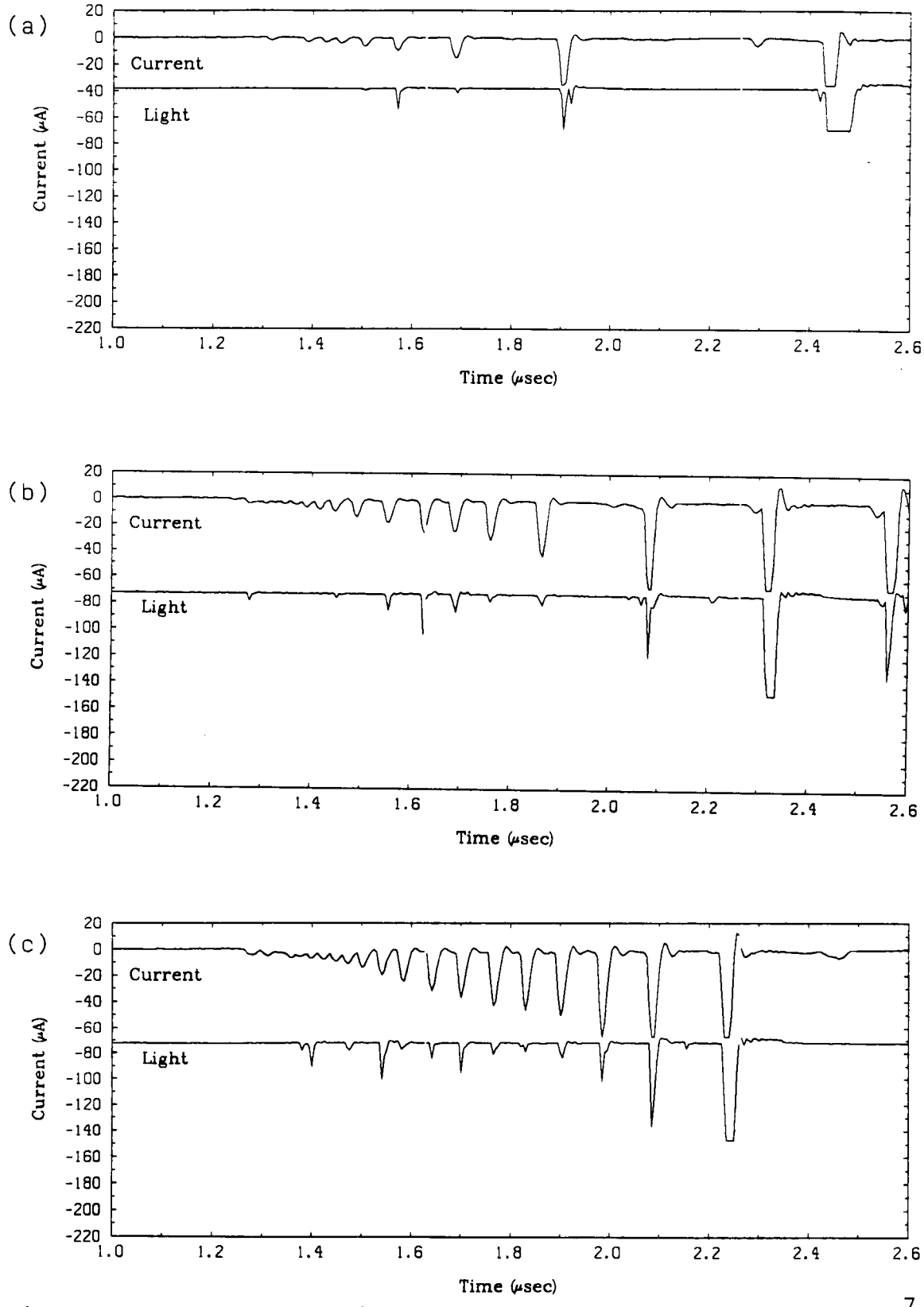

Fig. 12: Current and light pulses for a PMT gain of 2×10^7 at needle voltages of (a)-11 kV, (b)-13 kV, and (c)-15 kV

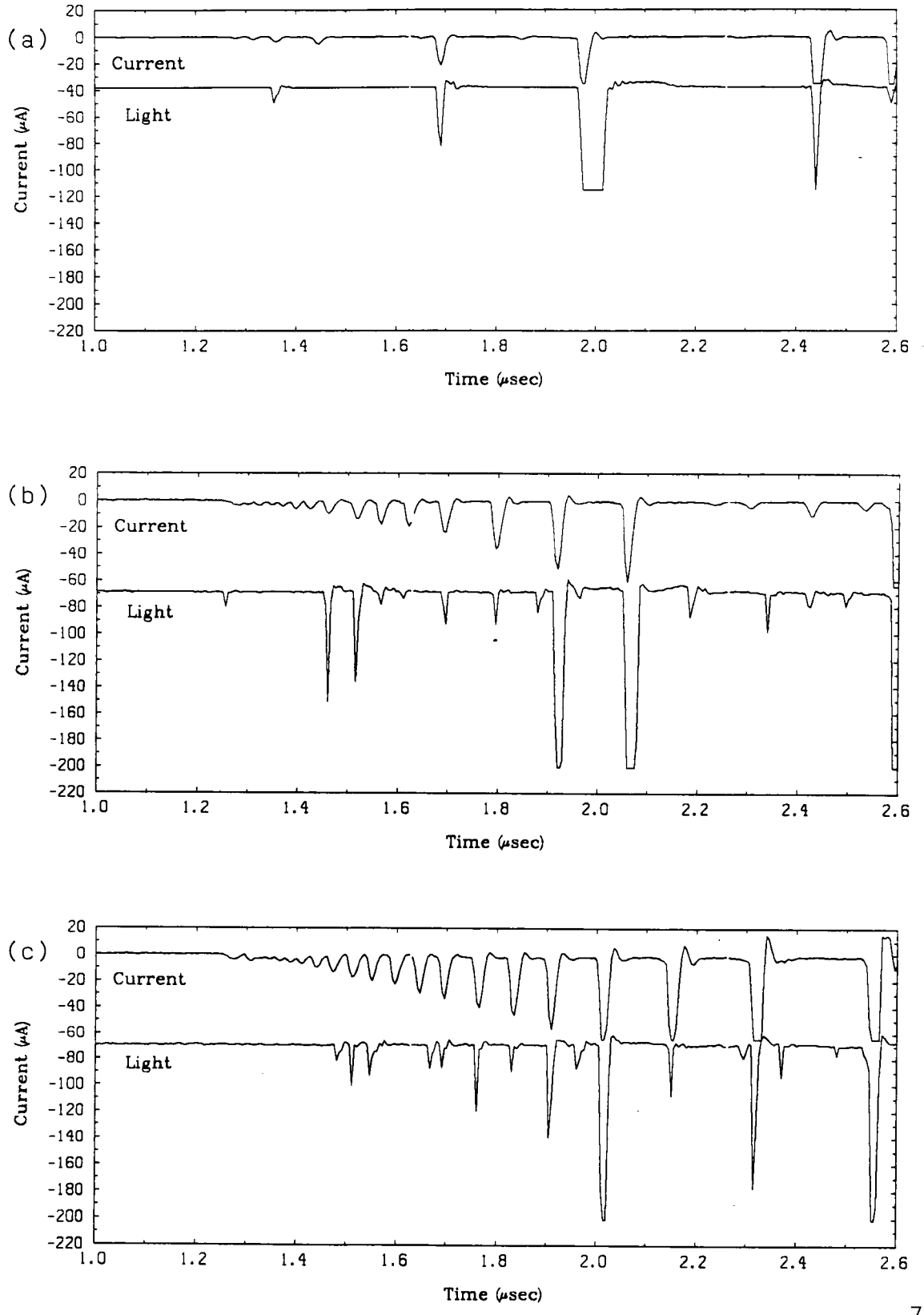

Fig. 13: Current and light pulses for a PMT gain of 4×10^7 at needle voltages of (a)-11 kV, (b)-13 kV, and (c)-15 kV

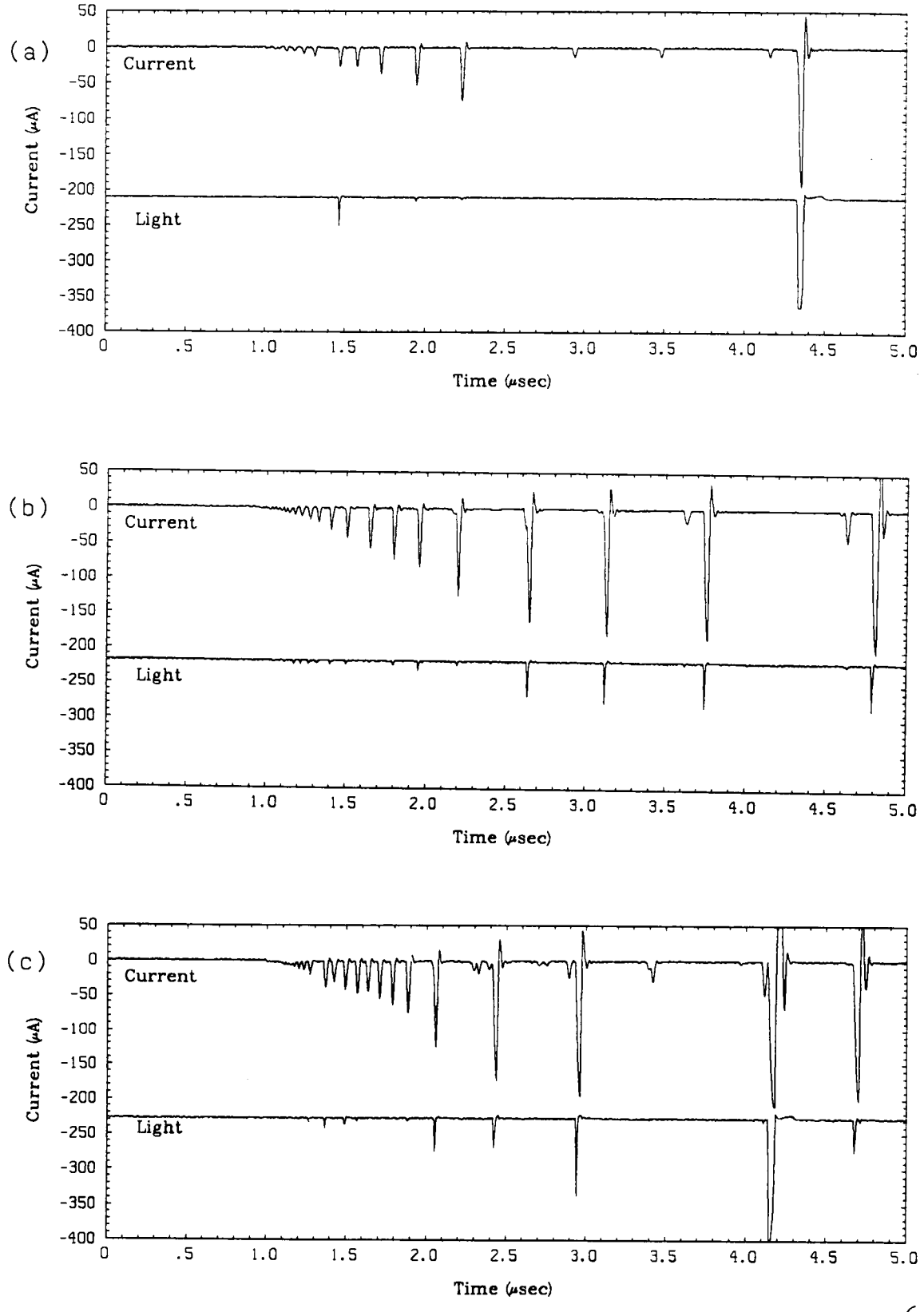

Fig. 14: Light and current pulses for a PMT gain of 5×10^6 at needle voltages of (a)-11 kV, (b)-13 kV, and (c)-15 kV

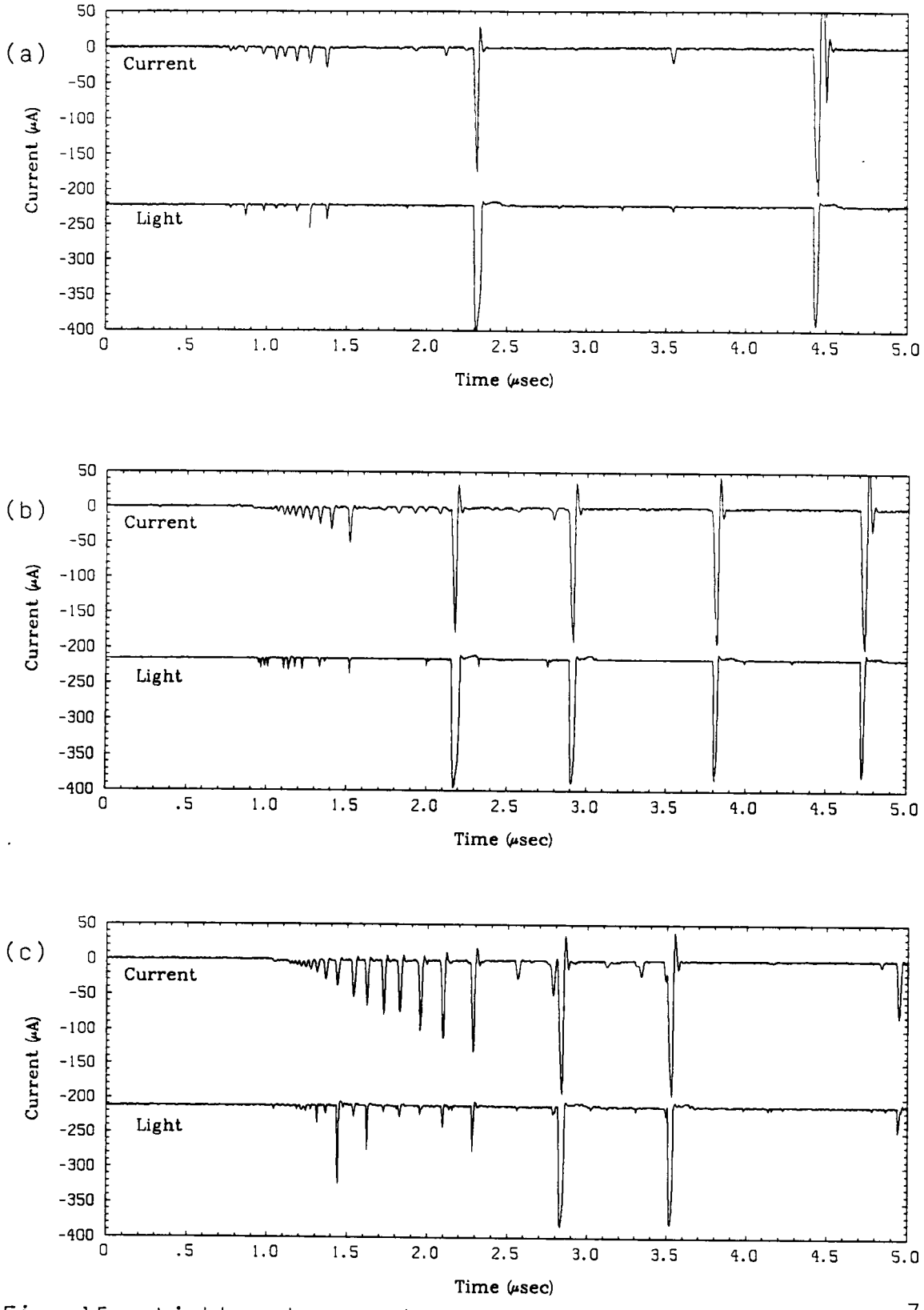

Fig. 15: Light and current pulses for a PMT gain of 2×10^7 at needle voltages of (a)-11 kV, (b)-13 kV, and (c)-15 kV

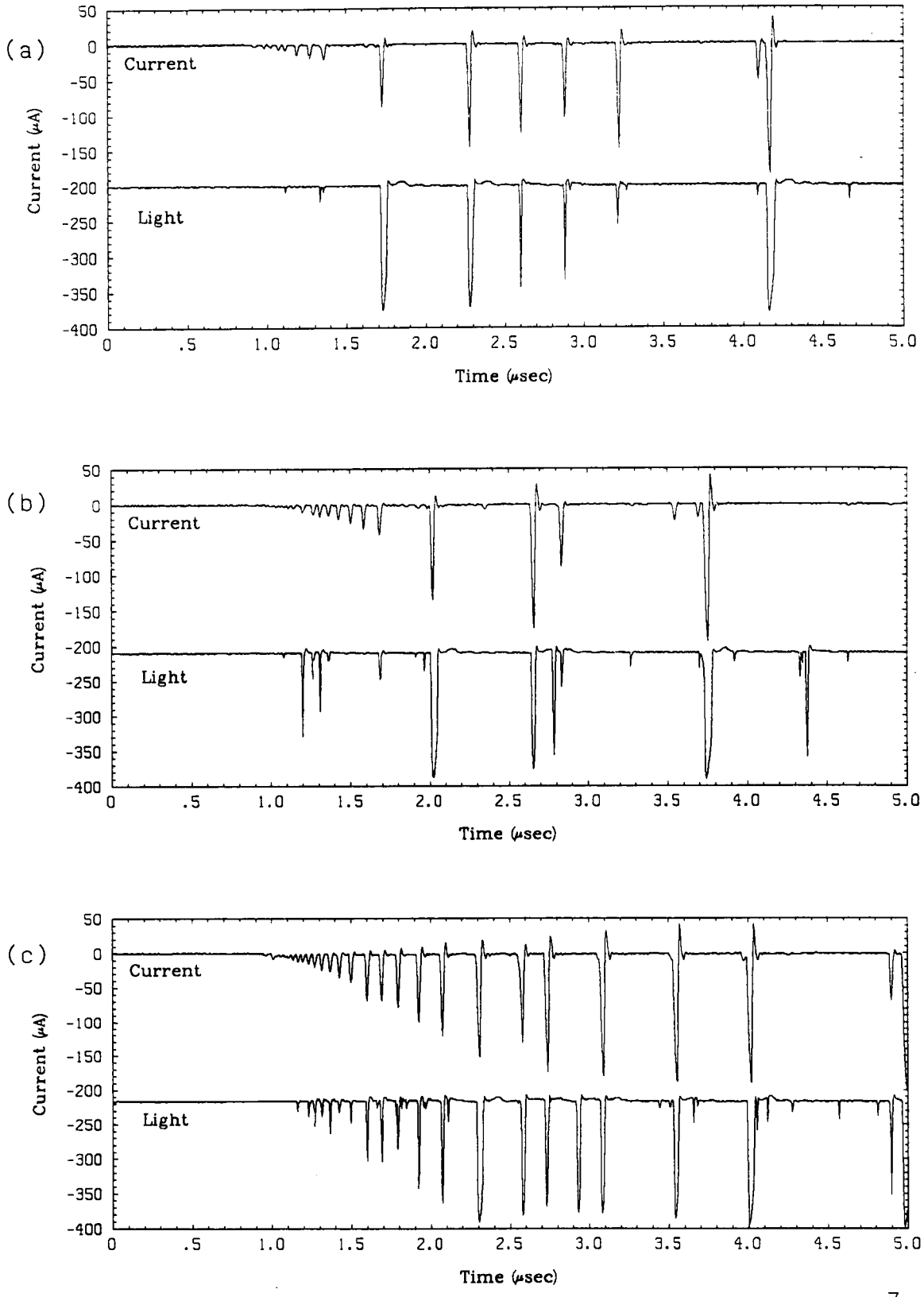

Fig. 16: Light and current pulses for a PMT gain of 4×10^7 at needle voltages of (a)-11 kV, (b)-13 kV, and (c)-15 kV

the peak ranged from 10 to 25 ns, while a light pulse was 5 to 50 ns wide. Not every current pulse produced a light pulse that was detectable, and the amplitudes of the current and light pulses were not well correlated. These two observations could be due to the fact that 1) the LDR does not develop on the same site of the needle every time as observed by Alexeff et al. [2], 2) the LDR acts as a lens that has a focal length that varies with its growth, 3) the spectral content of the LDR could vary with its growth affecting the PMT output through the spectral response of the cathode, and 4) the light might be emitted directionally instead of uniformly. In general, the amplitude of the current pulses and the width of the initial sequence that increases linearly with time were proportional to the needle high voltage.

Referring to the typical plot of prebreakdown current and light in Fig. 17, the apparent delay of the current and light pulses was defined as

$$t_a = t_{la} - t_{ca} \ . \qquad (4\text{-}1)$$

That is, the apparent delay was determined by finding the difference between the time the light took to reach 2% of its peak value and the time the current took to reach 2% of its peak value. The 2% level was used because it was the same level used in measuring the light detection delay t_{ld} (section 3.3.1) and the current detection delay t_{cd} (section 3.3.2). The real delay was defined as

$$t_r = t_{lr} - t_{cr} \ , \qquad (4\text{-}2)$$

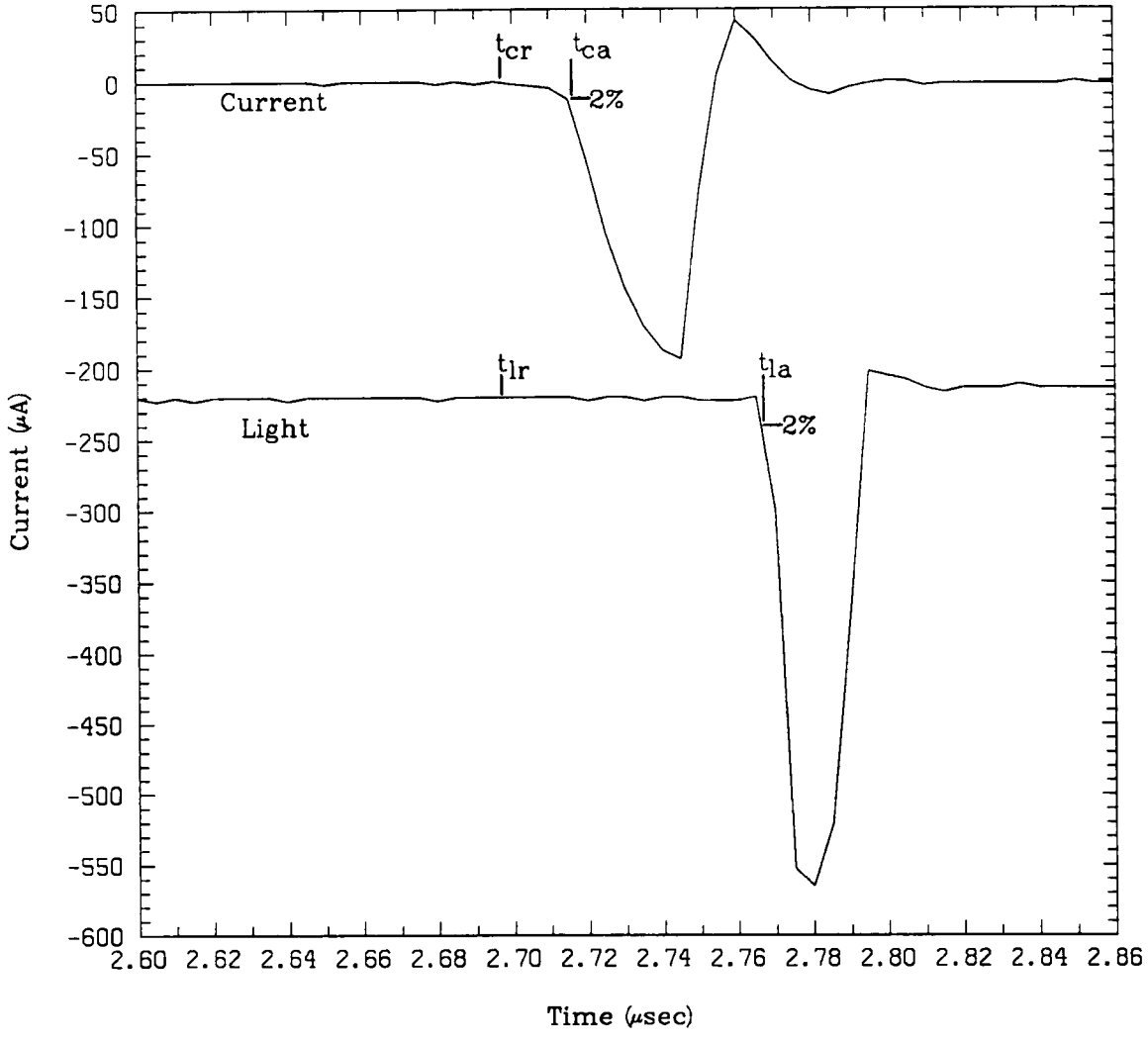

Fig. 17: Typical plot of a current and light pulse

where t_{lr} = actual time that the light reached 2% of its peak value,

and t_{cr} = actual time that the current reached 2% of its peak value.

Equation (4-2) can be rewritten in terms of the apparent delay and the measured detection delays as

$$t_r = t_a - t_{ld} + t_{cd} . \qquad (4\text{-}3)$$

The apparent delay was determined for each combination of needle high voltage and PMT gain as shown in Table 2. The values in this table are the averages and standard deviations calculated from a set of at least 18 measured apparent delays for each combination of high voltage and PMT gain. The last column on the right shows the average and standard deviation of all the measured apparent delays for a particular value of PMT gain. Note that in Table 2 the apparent delay decreases with increasing PMT gain as it should.

Table 2

Average and standard deviation of apparent delays

	Apparent delays (nanoseconds)			
PMT Gain	@ -11 kV	@ -13 kV	@ -15 kV	@ All HVs
5×10^6	54.2 $\pm$ 3.2	53.3 $\pm$ 4.0	52.7 $\pm$ 1.4	53.4 $\pm$ 3.1
2×10^7	51.2 $\pm$ 2.6	50.5 $\pm$ 2.5	50.4 $\pm$ 1.8	50.7 $\pm$ 2.3
4×10^7	49.3 $\pm$ 1.7	49.3 $\pm$ 2.2	48.9 $\pm$ 1.4	49.2 $\pm$ 1.8

The real delays in Table 3 were calculated from equation (4-3) using the same numbers used to determine the apparent delays in Table 2. The resolution of the values in Table 3 is limited by the effective sampling rate of 2.5 nanoseconds. These values suggest the possibility of the light lagging the current. This delay between the light and current could be attributed to the fact that a discharge in the LDR would excite the different molecules present. After some period of time, these molecules would revert back to their stable state and emit photons. The time an electron would take to change energy levels would depend on the characteristics of the molecule itself. The typical half-life of an excited state is 0.1 to 1.0 nanoseconds, but some states can exist for up to 1.0 microseconds [16]. Since the real delays were not constant for all PMT gains, an error could have been made in measuring the delays of the light detection system.

Table 3

Average and standard deviation of real delays

	Real delays (nanoseconds)			
PMT Gain	@ -11 kV	@ -13 kV	@ -15 kV	@ All HVs
5×10^6	2.2 $\pm$ 3.2	1.3 $\pm$ 4.0	0.7 $\pm$ 1.4	1.4 $\pm$ 3.1
2×10^7	5.2 $\pm$ 2.6	4.5 $\pm$ 2.5	4.4 $\pm$ 1.8	4.7 $\pm$ 2.3
4×10^7	6.3 $\pm$ 1.7	6.3 $\pm$ 2.2	5.9 $\pm$ 1.4	6.2 $\pm$ 1.8

4.3 Spectral Content of Prebreakdown Light Emission

The basic processing steps that were used in determining the intensity of the light spectrum at a specific wavelength are shown in Fig. 18. The impulse-like response of the monochromator sampled the light signal $x(t)$ at a specified wavelength α, resulting in the monochromatic signal $x'(t)$. The sensitivity of the PMT cathode and the gain of the PMT then transformed the signal $x'(t)$ into a current $i_1(t)$, which was digitally integrated using the Tektronix 4041 computer to give the value q_1. The prebreakdown current $i_2(t)$ was also integrated digitally to find the magnitude of the discharge q_2. Since this charge represented the amount of energy released in the LDR, it was used to normalize the value q_1 by dividing q_1 by q_2. The values q_1 and q_2 were summed over all the waveforms for a given wavelength, and then q_1 was divided by q_2 to give I_α, which was then compensated for the response of the PMT cathode (Fig. 19) [34] to give the final value of spectral intensity at the wavelength α. The integration step was used because the signals $x(t)$ and $i_2(t)$ were pulsed instead of continuous.

The signals $i_1(t)$ and $i_2(t)$ were integrated using a trapezoidal approximation as depicted in Fig. 20, where the magnitude of the time varying signal $y(t)$, at t equal to nT, was y_n. The area under any two consecutive data points, y_n and y_{n+1}, was

$$A_y = T(y_n + y_{n+1})/2 \ , \qquad (4\text{-}4)$$

where T was the sampling interval (5 nsec). Integrating

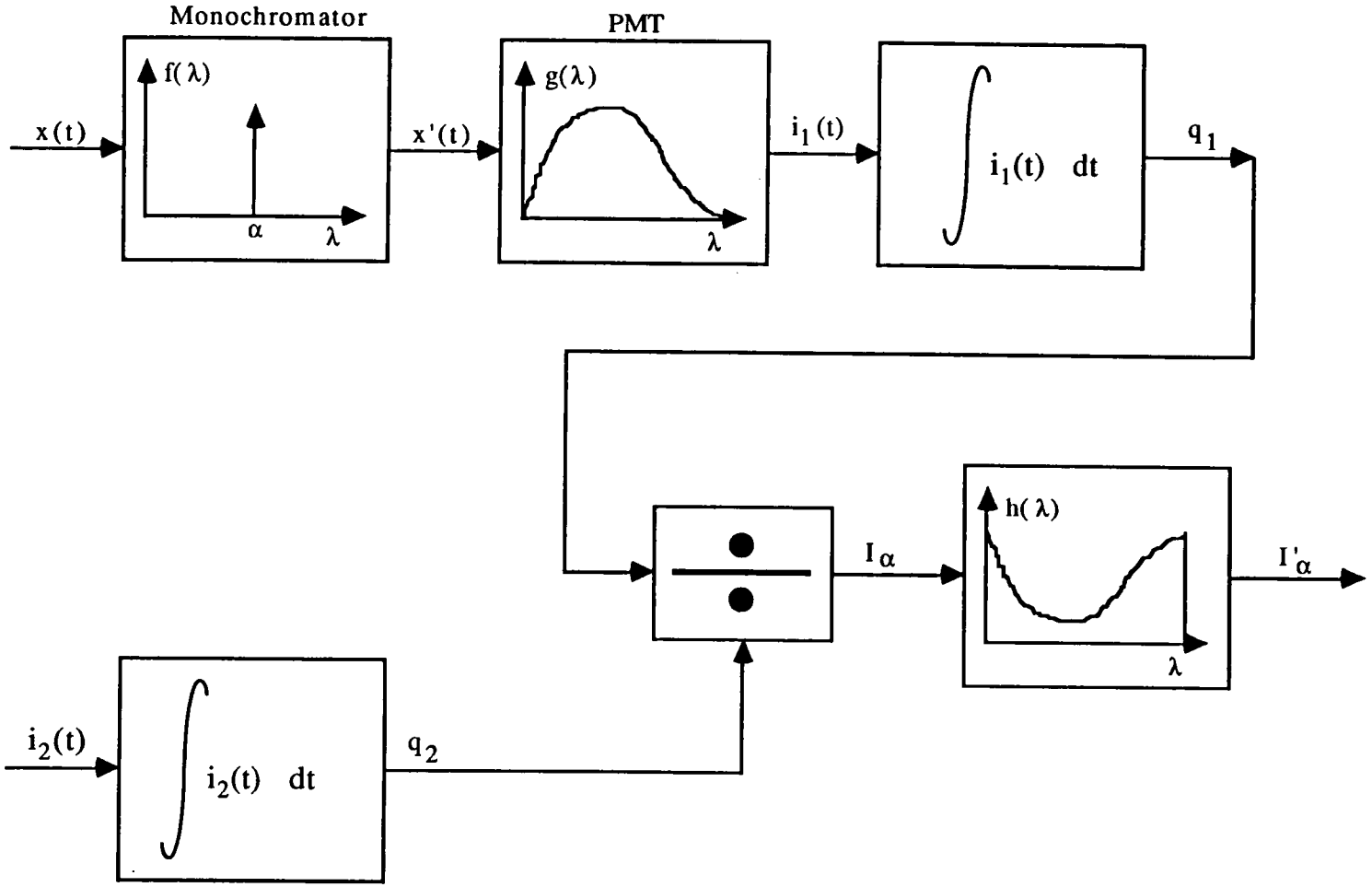

Fig. 18: Block diagram of processing used to determine the spectral intensity at a specified wavelength

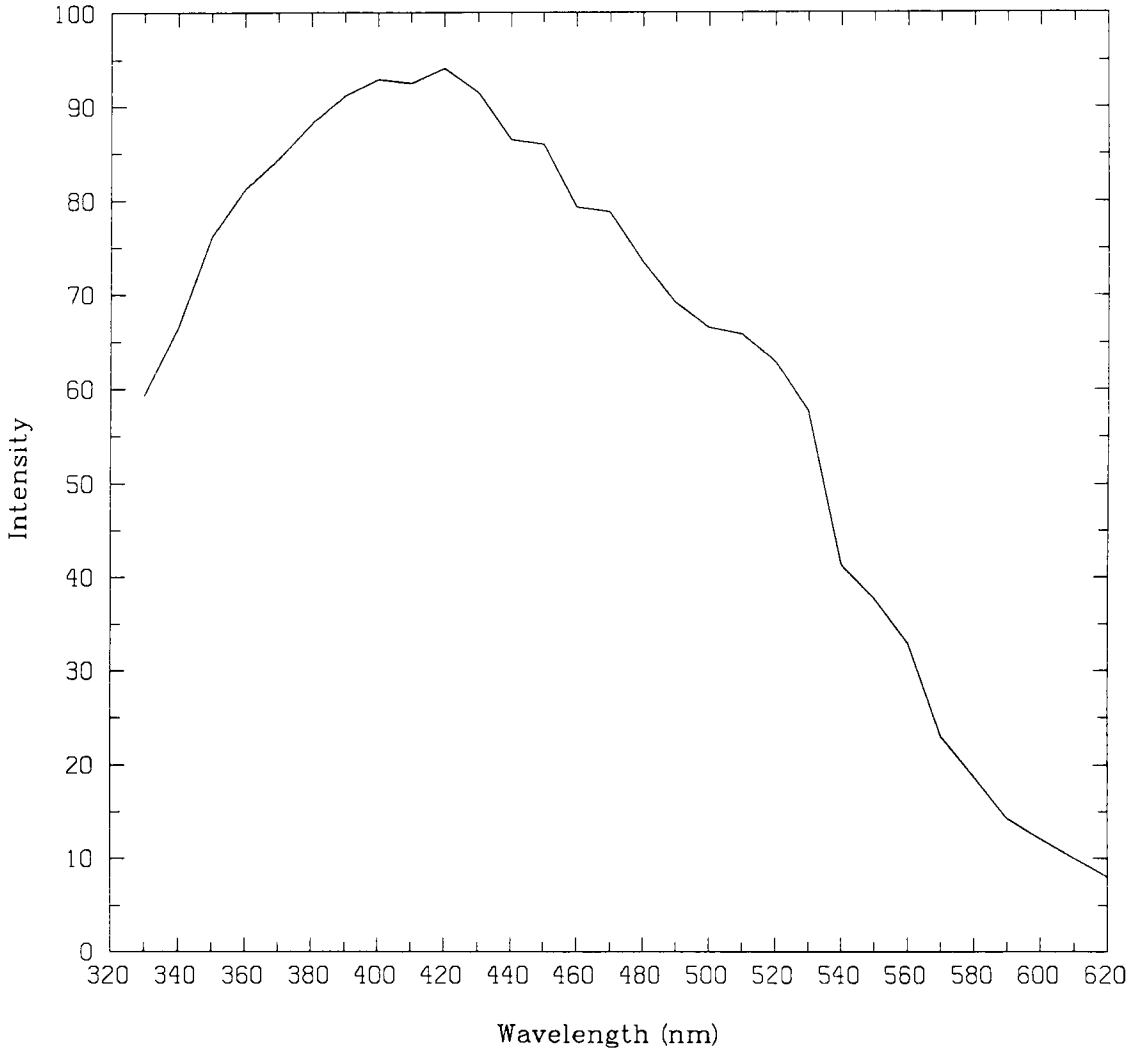

Fig. 19: Spectral response of PMT cathode

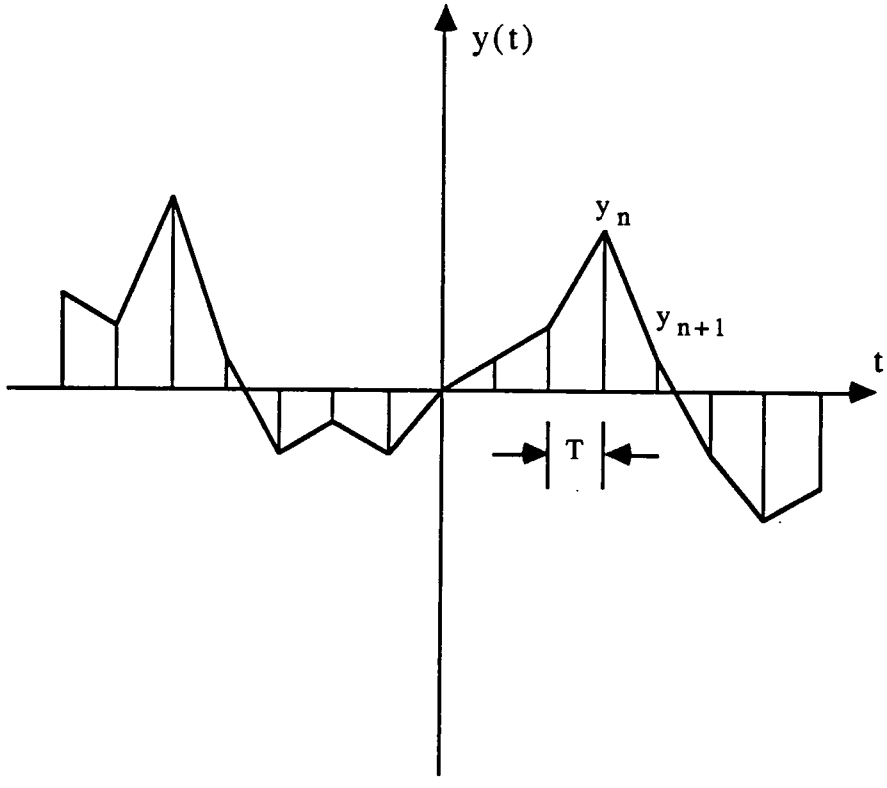

Fig. 20: Integration of waveform using trapezoidal approximation

over a portion of the waveform from n equal N1 to N2 resulted in the sum

$$T/2 \sum_{n=N1}^{N2} (y_n + y_{n+1}) \quad . \qquad (4\text{-}5)$$

Rearranging this sum gave

$$T/2((2*\sum_{n=N1}^{N2} y_n) - y_{N1} - y_{N2}) \quad , \qquad (4\text{-}6)$$

which was incorporated into a computer program that would integrate the waveforms that were stored on disk.

The light emission spectra in Figs. 21, 22, 23, 24, 25, and 26 were obtained from the processing of 15, 20, 25, 30, 35, and 40 waveform pairs of light and current at each wavelength respectively. Each spectrum contains the information that was used to generate the previous spectrum. For example, the spectrum plotted in Fig. 26 was obtained from processing the 35 waveform pairs used in producing the spectrum in Fig. 25 plus 5 new waveform pairs. Peaks at 430, 510, and 590 nm were in all of these spectra. In all but the first spectrum, a peak at 480 nm was present. The strong peak at 430 nm could be due to hydrocarbon reactions like those found in the sun's atmosphere which produce an intense band at 431.25 nm [7]. The peak detected at 590 nm could be associated with hydrocarbons under high pressure that produce spectral peaks at 468.0 and 589.9 nm [7]. Other hydrocarbon peaks at 360.7 and 410.2 nm were not observed. Peaks in the hydrocarbon "swan" band at 436.5, 473.7, and 516.5 [7] would not have been detected because the bandpass of the monochromator was only 5 nm. The energy difference that an electron experiences as it changes states determines the wavelength of the photon emitted. This

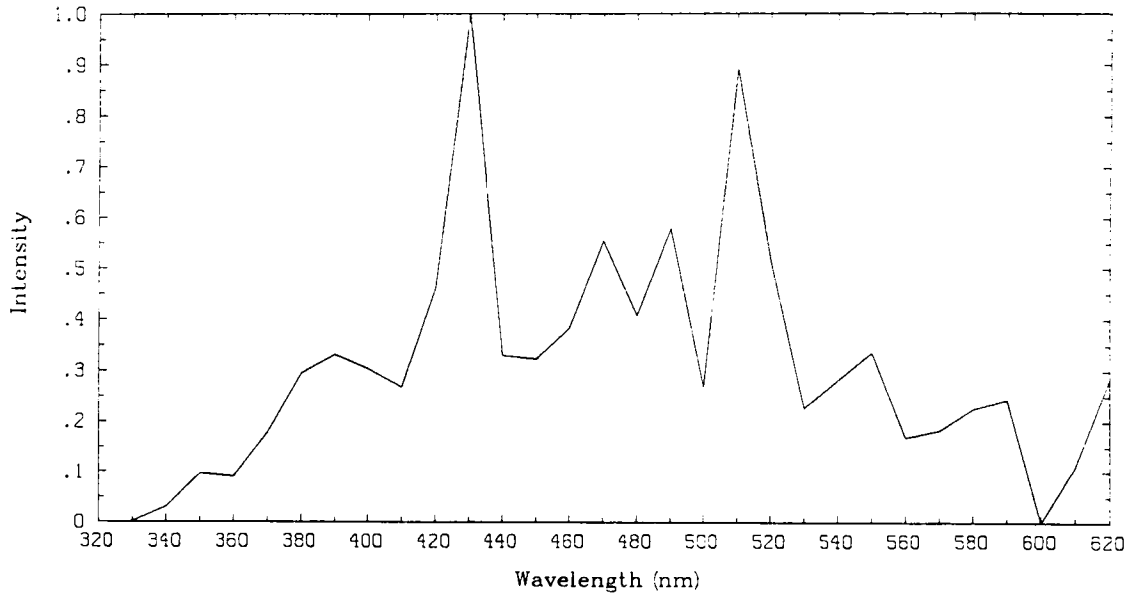

Fig. 21: Light emission spectrum after processing 15 waveform pairs

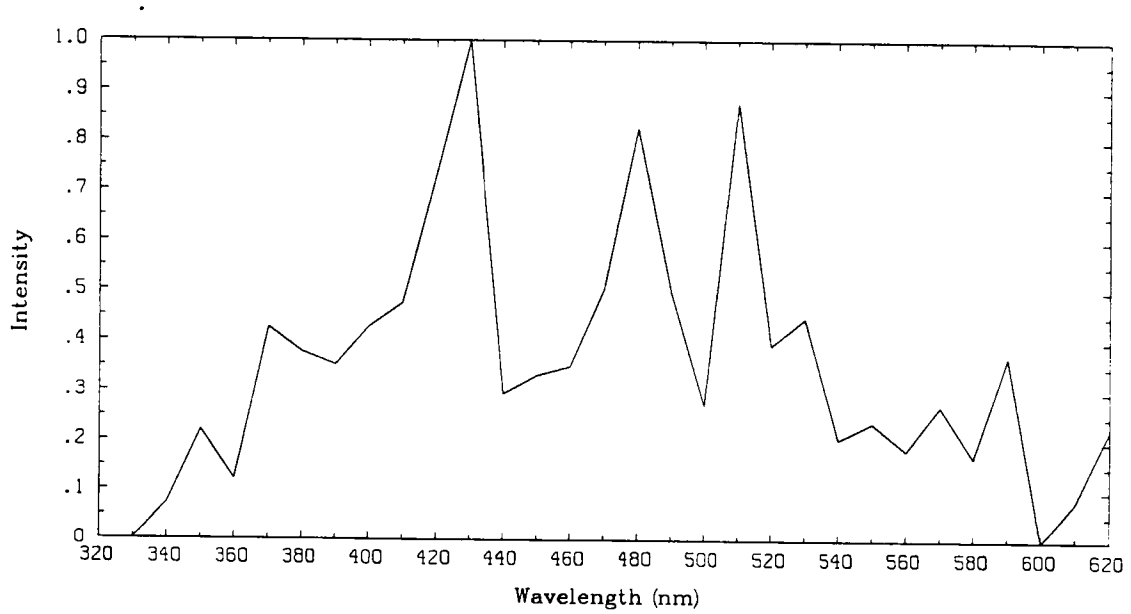

Fig. 22: Light emission spectrum after processing 20 waveform pairs

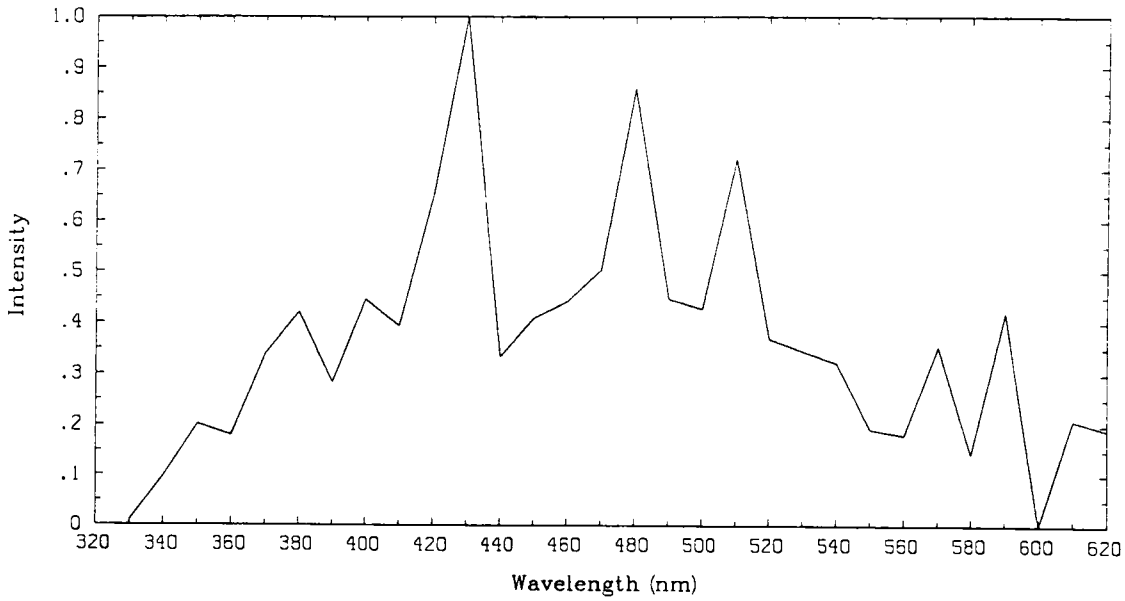

Fig. 23: Light emission spectrum after processing 25 waveform pairs

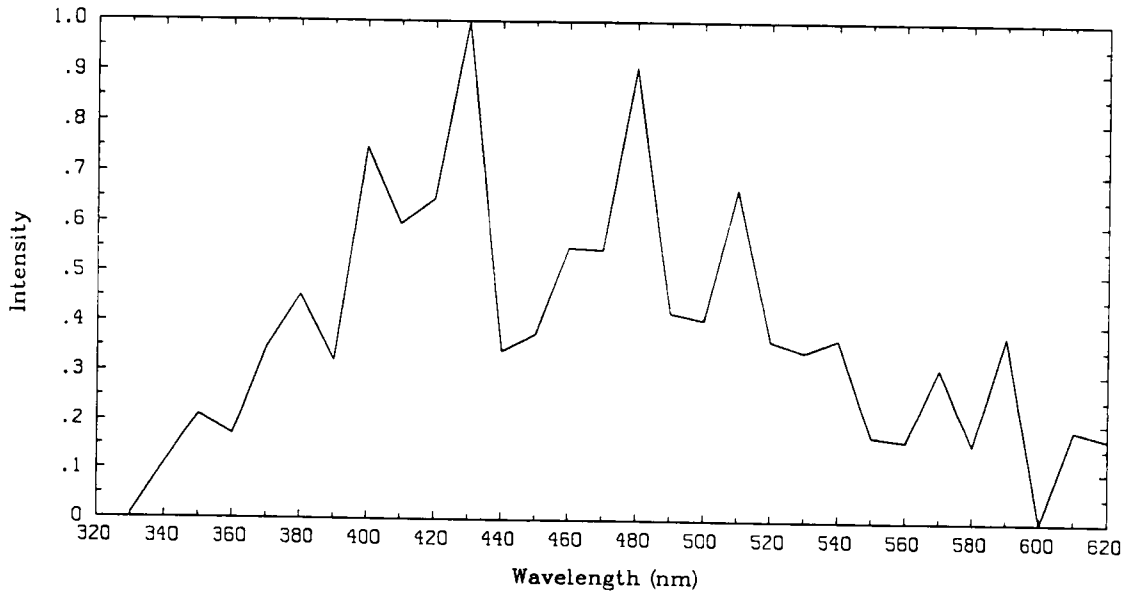

Fig. 24: Light emission spectrum after processing 30 waveform pairs

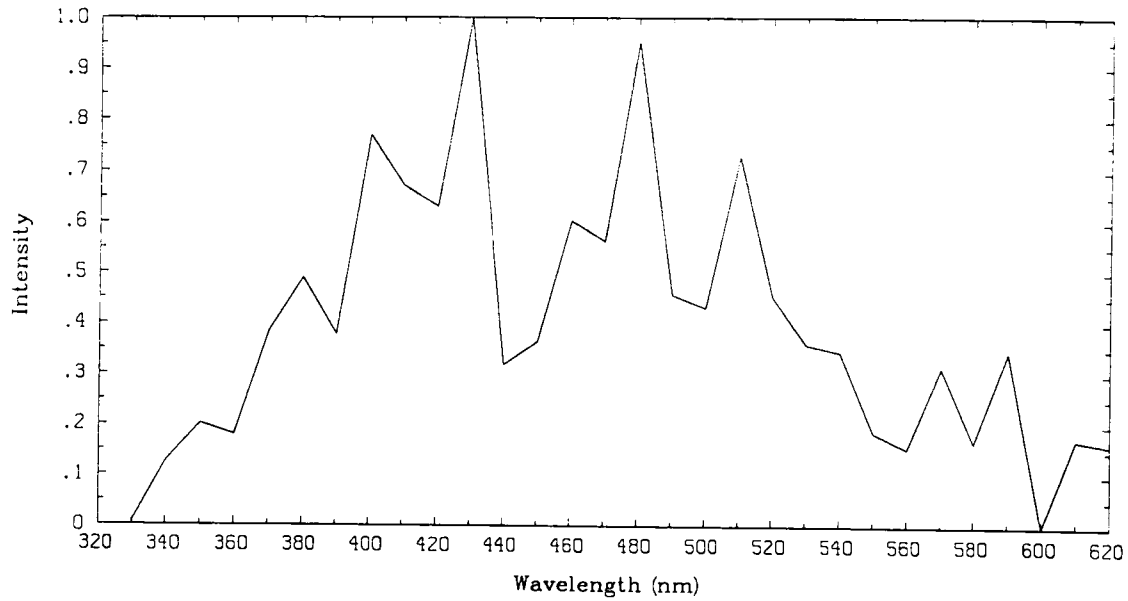

Fig. 25: Light emission spectrum after processing 35 waveform pairs

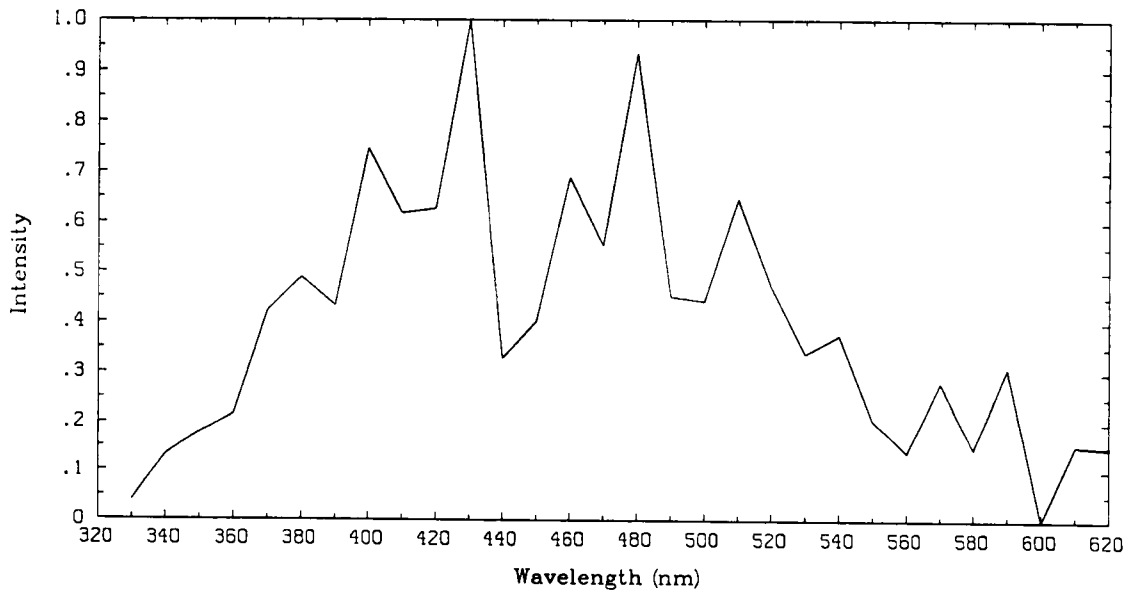

Fig. 26: Light emission spectrum after processing 40 waveform pairs

relationship is given by [15]

$$\lambda = hc/\Delta E \ , \qquad (4\text{-}7)$$

where h = Planck's constant (4.14×10^{-15} eV-sec),

c = speed of light (3×10^{8} m/sec)

and ΔE = change in energy (eV) .

The changes in energy required for the spectral peaks at 430, 510, and 590 nm are 2.89, 2.43, and 2.11 eV respectively.

The measurements made at some of the wavelengths were not consistent as shown in the previous figures. This inconsistency could have been due to the following phenomenon. The monochromator was calibrated so that the spectral response was essentially a 5 nm wide rectangle centered at the chosen wavelength α provided that the focused source filled the entire slit as shown in Fig. 27. Assuming that the source was focused so that it filled only the left half of the slit, the effective width of the slit would be halved. This alignment would increase the spectral resolution and shift the center wavelength as pictured in Fig. 28. In this case, an actual peak in the spectrum of the source at ω would have been detected. If the source were refocused so that it only filled the right half of the slit, the spectral line at ω would not be detected as depicted in Fig. 29. This measurement error probably occurred since the focused size of the LDR probably did not fill the entrance slit in this setup.

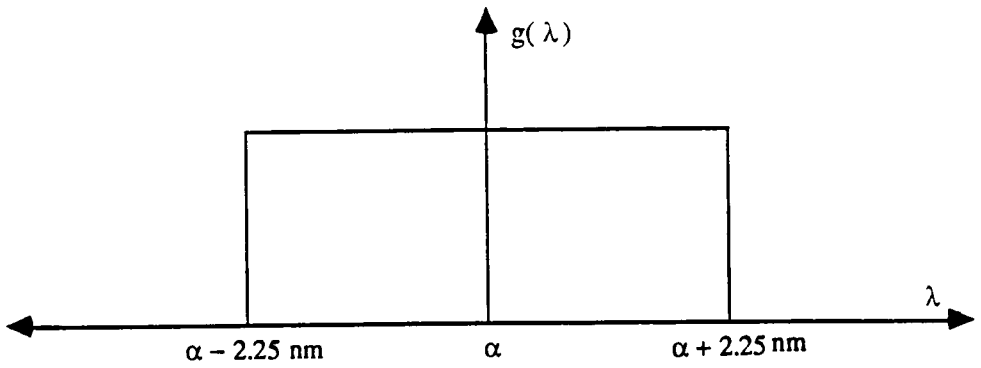

Fig. 27: Effective spectral response of monochromator

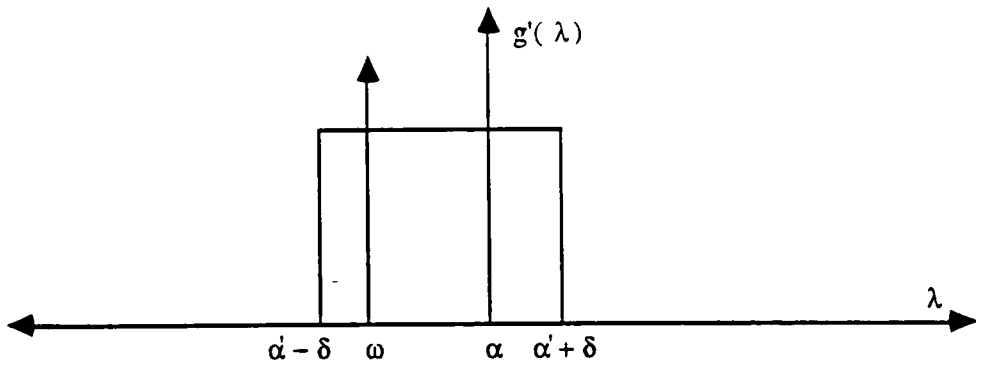

Fig. 28: Effective spectral response of monochromator when source is focused on left half of slit

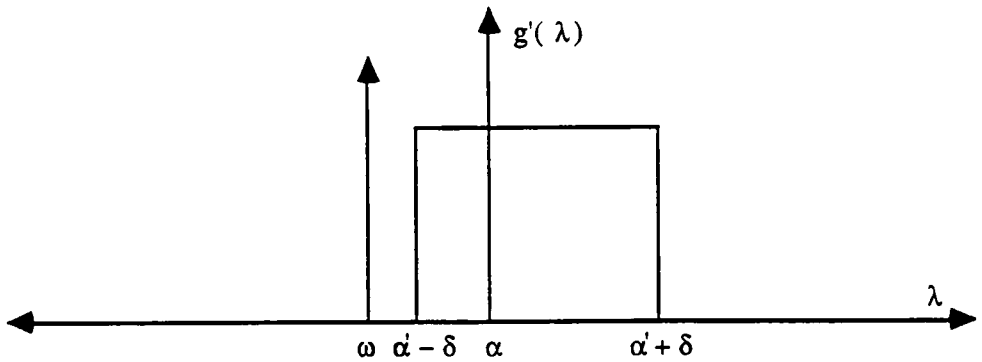

Fig. 29: Effective spectral response of monochromator when source is focused on right half of slit

CHAPTER 5

CONCLUSION

5.1 Summary of Results

The major accomplishments of this research were the determination of the temporal correlation of prebreakdown current and light and the measurement of the spectrum of the prebreakdown light emission. Neither of these accomplishments have previously been reported.

The results of the temporal correlation study suggest that a prebreakdown current pulse actually leads the light pulse that it generates by 1 to 6 nanoseconds. However, better time resolution measurements are needed to determine if this result is correct. The time delay between the two signals may depend on the characteristics of the molecules that are excited into higher energy states, such as the types of electron orbits not normally occupied. Therefore, better resolution techniques could provide information that could be used to determine these characteristics.

A method was developed to determine the spectral content of prebreakdown light emission, which had never been measured before. The light emission spectrum was found to be very structured. The peaks in the spectrum corresponded to hydrocarbon reactions like those found in the sun's atmosphere and to hydrocarbons under high pressure.

5.2 Suggestions for Future Research

One major improvement that could be made to both of the studies reported in this thesis would be to construct a test cell where the viewport was mounted much closer to the needle. This modification would allow a lens to be placed much closer to the needle, which would improve the light gathering capability of the system, allowing smaller light pulses to be detected.

To further improve the detection capability and to also include the ultraviolet region in the spectral study, a tube filled with helium gas could be added to connect the viewport, lens, and monochromator/PMT. The lens would have to transmit ultraviolet, and the monochromator would also have to be filled with helium. An alternative to filling the tube with helium would be to evacuate the tube.

To correctly interpret the structure of the light emission spectrum, more data should be taken using smaller wavelength intervals than 10 nm.

Since the spectrum of the prebreakdown light emission depends on the molecules present in the LDR and their density, which could vary with the growth of the LDR, a measurement of the spectrum versus LDR growth should be made. A multichannel spectrum analyzer in conjunction with an image intensifier would prove useful in this study. To verify the presence of certain gases evolved in the prebreakdown process, a mass spectrometer could be connected to the test cell.

LIST OF REFERENCES

References

[1] I. Alexeff, T. V. Blalock, A. L. Wintenberg, J. V. Foust, and M. O. Pace, "Multipulse Prebreakdown Phenomena in Liquid Dielectrics", Proceedings of the 14th International Conference on Plasma Science, p. 55, 1987.

[2] I. Alexeff, A. L. Wintenberg, D. N. Pittman, M. O. Pace, F. F. Dyer, and M. S. Radar, "Self-Luminous, Prebreakdown Phenomena in Liquid Hexane", 1988 Annual Report of the Conference on Electrical Insulation and Dielectric Phenomena, 1988.

[3] A. Beroual and R. Tobazeon, "Prebreakdown Phenomena in Liquid Dielectrics", IEEE Transactions on Electrical Insulation, Vol. EI-21, No. 4, pp.613-627, 1986.

[4] T. V. Blalock, "Low-Noise Wideband Amplification System for Acquiring Prebreakdown Current Pulses in Liquid Dielectrics", IEEE Transactions on Electrical Insulation, (To be published.)

[5] R. Coelho and J. Debeau, "Properties of the Tip-Plane Configuration", Journal of Physics D: Applied Physics, Vol. 4, pp. 1266-1280, 1971.

[6] J. C. Devins, S. J. Rzad, and R. J. Schwabe, "Breakdown and Prebreakdown Phenomena in Liquids", Journal of Applied Physics, Vol. 52, No. 7, pp. 4531-4545, 1981

[7] W. G. Driscoll, Handbook of Optics, McGraw-Hill, Inc., New York, Section 11, 1978.

[8] G. J. FitzPatrick and E. O. Forster, "The Effect of Pressure on the Prebreakdown Events in Toluene", 1986 Annual Report of the Conference on Electrical Insulation and Dielectric Phenomena, pp. 299-303, 1986.

[9] G. J. FitzPatrick, and E. O. Forster, "In Search of a Relation Between Streamers and Partial Discharges in Condensed Matter", Conference Record of the 1988 IEEE International Symposium on Electrical Insulation, pp. 23-26, 1988.

[10] G. J. FitzPatrick, E. O. Forster, R. E. Hebner, and E. F. Kelley, "Prebreakdown Cathode Processes in Liquid Hydrocarbons", IEEE Transactions on Electrical Insulation, Vol. EI-22, No. 4, pp. 453-458, 1987.

[11] E. O. Forster and P. P. Wong, "High Speed Schlieren Studies of Electrical Breakdown in Liquid Hydrocarbons", IEEE Transactions on Electrical Insulation, Vol. EI-12, No. 6, pp. 435-442, 1977.

[12] E. O. Forster and P. P. Wong, "The Dynamics of Electrical Breakdown in Liquid Hydrocarbons, V. Light Emission Processes", Conference Record of the 1980 IEEE International Symposium on Electrical Insulation, pp. 222-224, 1980.

[13] E. O. Forster, "The Metal/Liquid Interface: The Charge Injection Process", IEEE Transactions on Electrical Insulation, Vol. EI-19, No. 6, pp. 524-528, 1984.

[14] E. O. Forster, "Progess in the Field of Electrical Breakdown in Dielectric Fluids", Proceedings of the Symposium on Dielectric Phenomena in Honor of the 70th Birthday of Professor Robert H. Cole, pp. 7-12, 1985.

[15] D. Halliday and R. Resnick, Fundamentals of Physics, John Wiley and Sons, Inc., New York, Chapter 39, 1981.

[16] H.H Jaffe and Milton Orchin, Theory and Applications of Ultraviolet Spectroscopy, John Wiley and Sons, Inc., New York, Chapter 19, 1962.

[17] M. C. Hanna, J. E. Thompson, and T. S. Sudarshan, "The Simultaneous Measurement of Light and Current Pulses in Liquid Dielectrics", 1983 Annual Report of the Conference on Electrical Insulation and Dielectric Phenomena", pp. 245-250, 1983

[18] R. E. Hebner, E. F. Kelley, E. O. Forster, and G. J. Fitzpatrick, "Observation of Prebreakdown and Breakdown Phenomena in Liquid Hydrocarbons", Journal of Electrostatics, Vol. 12, pp. 265-283, 1982.

[19] E. F. Kelley and R. E. Hebner, Jr., "The Electric Field Distribution Associated with Prebreakdown Phenomena in Nitrobenzene", Journal of Applied Physics, Vol. 52, No. 1, pp. 191-194, 1981.

[20] E. F. Kelley and R. E. Hebner, "Electro-Optic Field Measurement at a Needle Tip and Streamer Initiation in Nitrobenzene", 1986 Annual Report of the Conference on Electrical Insulation and Dielectric Phenomena, pp. 272-277, 1986.

[21] E. F. Kelley, R. E. Hebner, G. J. FitzPatrick and E. O. Forster, "The Effect of Pressure on Streamer Initiation in n-Hexane", Conference Record of the 1986 IEEE International Symposium on Electrical Insulation, pp. 66-68, 1986.

[22] E. F. Kelley, M. Nehmadi, R. E. Hebner, P. J. McKenney, and E. O. Forster, "Simultaneous Measurement of Light Emission, Current Pulses, and Growth of Prebreakdown Streamers in Hexane", 1987 Annual Report of the Conference on Electrical Insulation and Dielectric Phenomena, pp. 132-137, 1987.

[23] E. F. Kelley, M. Nehmadi, and R. E. Hebner (NBS), M. O. Pace, A. L. Wintenberg, T. V. Blalock, and J. V. Foust (UT), "Measurement of Partial Discharges in Hexane under DC Voltage", IEEE Transactions on Electrical Insulation, (To be published.)

[24] E. Morikawa, "Optical Observations of Prebreakdown Phenomena in Dielectric Oil", Electrical Engineering in Japan, Vol. 92, No. 1, pp. 11-17, 1972.

[25] J. K. Nelson, and P. B. McGrath, "Evidence for Transistions in the Prebreakdown Mechanism of Liquid Dielectrics", Proceedings of the IEEE, Vol. 122, No. 12, pp. 1439-1442, 1975.

[26] M. O. Pace, D. N. Pittman, A. L. Wintenberg, I. Alexeff, and T. V. Blalock, "Effects of Pressure Near One Atmosphere on Prebreakdown Current Pulses at a Needle Cathode in Hexane", Conference Record of the 1988 IEEE International Symposium on Electrical Insulation, pp. 23-26, 1988.

[27] M. O. Pace, I. Alexeff, A. L. Wintenberg, T. V. Blalock, J. V. Foust, and A. G. Bokil, "Theoretical Model for Initial Prebreakdown Current Pulses and Low Density Region at a Point Cathode in a Liquid Dielectric", (To be published.)

[28] A. Papoulis, Probability, Random Variables, and Stochastic Processes, McGraw-Hill, Inc., New York, pp. 54-58, 1984.

[29] R. L. Ramey, Physical Electronics, Wadsworth Publishing Company, Inc., Belmont, California, Section 5.10, 1961.

[30] S. Sakamoto and H. Yamada, "Optical Study of Conduction and Breakdown in Dielectric Liquids", IEEE Transactions on Electrical Insulation, Vol. EI-15, No. 3, pp. 171-181, 1980.

[31] J. A. R. Samson, Techniques of Ultraviolet Spectroscopy, John Wiley and Sons, Inc., New York, Chapters 2-3, 1967.

[32] A. H. Sharbough, J. C. Devins, and S. J. Rzad, "Progess in the Field of Electrical Breakdown in Dielectric Liquids", IEEE Transactions on Electrical Insulation, EI-13, 249-276, 1978.

[33] W. R. L. Thomas, "Computer Simulation of Electrical Breakdown in Dielectric Liquids", 1974 Annual Report of the Conference on Electrical Insulation and Dielectric Phenomena, pp. 540-548, 1974.

[34] Thorn EMI Gencom Inc., "Photomultipliers", Manual P001/F82, p. 20

[35] P. K. Watson, "EHD Instabilities in the Breakdown of Point-Plane Gaps in Insulating Liquids", 1981 Annual Report of the Conference on Electrical Insulation and Dielectric Phenomena, pp. 371-376, 1981.

[36] A. L. Wintenberg, M. O. Pace, T. V. Blalock, and J. V. Foust, "Statistics of Prebreakdown Current Pulses in n-Hexane", 1986 Annual Report of the Conference on Electrical Insulation and Dielectric Phenomena, pp. 293-298, 1986.

[37] A. L. Wintenberg, M. O. Pace, T. V. Blalock, and J. V. Foust, "Nonuniform Field Prebreakdown Current Pulses in Negatively Stressed n-Hexane", 1987 Annual Report of the Conference on Electrical Insulation and Dielectric Phenomena, pp. 95-100, 1987.

[38] A. L. Wintenberg, M. O. Pace, and T. V. Blalock, "Low-Noise, High-Bandwidth Amplification of Prebreakdown Current Pulses in Liquid Dielectrics", Conference Record of the 1988 IEEE International Symposium on Electrical Insulation, pp. 383-384, 1988.

[39] A. L. Wintenberg, M. O. Pace, and T. V. Blalock, "Prebreakdown Current Pulses in n-Hexane and other Dielectric Fluids", IEEE Transactions on Electrical Insulation, (To be published.)

[40] P. P. Wong and E. O. Forster, "The Dynamics of Electrical Breakdown in Liquid Hydrocarbons", IEEE Transactions on Electrical Insulation, Vol. EI-17, No. 3, pp. 203-220, 1982.

[41] H. Yamashita and H. Amano, "Prebreakdown Current and Light Emission in Transformer Oil", IEEE Transactions on Electrical Insulation, Vol. EI-20, No. 2, pp. 247-255, 1985

VITA

Donald Neal Pittman was born in Nashville, Tennessee on January 3, 1964. He attended elementary school in that city and then moved to White House, Tennessee in 1976, where he graduated from White House High School in June 1982. After entering The University of Tennessee at Martin in September 1982 and then transferring to The University of Tennessee at Knoxville in September 1984, he received a Bachelor of Science degree in Electrical Engineering in June 1987. Continuing his eduacation, he reentered The University of Tennessee at Knoxville that summer and began study toward a Master's degree in Electrical Engineering. This degree was awarded in December 1988.

The author is a member of Tau Beta Pi National Engineering Honor Society, Eta Kappa Nu Electrical Engineering Honor Society, and the Institute of Electrical and Electronics Engineers. Mr. Pittman will be employed by System Dynamics, Inc. in Hunstville, Alabama, beginning in September 1988.